6-5-2017

Static Testing of Propulsion Elements for Small Multirotor Unmanned Aerial Vehicles

Robert W. Deters
Embry-Riddle Aeronautical University, DETERSR1@erau.edu

Stefan Kleinke
Embry-Riddle Aeronautical University, kleinkes@erau.edu

Michael S. Selig
University of Illinois, m-selig@illinois.edu

Static Testing of Propulsion Elements for Small Multirotor Unmanned Aerial Vehicles

Robert W. Deters,* Stefan Kleinke,†
Embry-Riddle Aeronautical University - Worldwide, Daytona Beach, FL 32114

and Michael S. Selig‡
University of Illinois at Urbana-Champaign, Urbana, IL 61801

The growing use of small multirotor aircraft has increased the interest in having better performance results especially with the propulsion system. The size of the propellers used on these aircraft operate at low Reynolds numbers that are typically less than 200,000. Static performance testing of ten propeller pairs (tractor and pusher) were completed and is the beginning of a systematic test of propellers used on multirotor systems. The propellers chosen for this initial set of tests were selected from four popular quadrotors. Besides testing the propellers provided with the aircraft, propellers that are sold as replacements from third-party companies were also tested. Both the 3D Robotics Solo and DJI Phantom 3 had multiple propellers tested and a method to compare the resulting endurance is discussed.

I. Introduction

Given the recent rapid rise in the application of Small Unmanned Aerial Systems (sUAS) for recreational, commercial, and research uses[1] and the expected further growth for their use in a variety of sectors such as precision agriculture, infrastructure inspection, transportation, and emergency services,[2–4] it is somewhat surprising on the limited amount of data available about the systems and whether the data can reliably describe the performance.[5,6] The Federal Aviation Administration (FAA) defines a sUAS as an aircraft that weighs less than 55 lb and has no provision for human intervention from within.[7] An increase in use of sUAS has been seen especially since 14 CFR part 107 provides the framework for widespread commercial application in the U.S.[1,7,8] The number of owner registrations of consumer- and prosumer-grade drones have increased to over 626,000 as of December 31, 2016,[1] up from nearly 300,000 registrations during the first 30 days of the registration requirement just a year prior.[9] The FAA estimates that there are around 1.1 million individual drones in the U.S. for distinctly hobby and recreational uses alone. Globally, these increases in usage were mirrored, and among sUAS platforms, partly based on availability and partly due to ease of operation and usefulness for the intended application, multirotor platforms dominate the sUAS landscape.[3]

Traditional aircraft performance evaluation, which is predominantly based on over a century of manned aircraft engineering, design, and testing, can only limitedly help to predict the performance characteristics of sUAS. The conventional literature on aircraft performance (e.g., Anderson,[10] Dole et al.,[11] Hale,[12] Hurt,[13] and McCormick[14]), primarily focus on large-scale fixed-wing aircraft, and literature on vertical take-off and landing primarily focuses on full-scale single-rotor helicopters (e.g., U.S. Army,[15] FAA,[16] Hurt,[13] and McCormick[17]). Typical performance criteria, such as range, endurance, and maximum gross weight, are usually based on a fuel consuming engine while electrical propulsion is very common with sUAS. The small size of sUAS also adds the complexity of being in the low Reynolds number regime. Typical propeller diameters for sUAS (both fixed-wing and multirotor systems) range from only a couple of inches to diameters of over 16 in. The size of these rotors can result in operational Reynolds numbers of less than 200,000.[18,19]

*Assistant Professor, Department of Engineering and Technology, AIAA Member.
†Assistant Professor, Department of Aeronautics, Undergraduate Studies.
‡Professor, Department of Aerospace Engineering, AIAA Associate Fellow.

Airfoils operating in low Reynolds numbers typically see a decrease in lift and an increase in drag.[20–26] Since propeller thrust is largely dependent on the lift and power is largely dependent on the drag, the efficiency of small-scale propellers is highly influenced by the Reynolds number. The low Reynolds numbers also make predicting the performance of the propellers difficult.[27–30] Therefore, performance prediction of these unmanned aircraft is difficult due to their small size, and design and application considerations are rather based on a trial-and-error type evaluation of a specific platform for a specific purpose.

There is a lack of standardization in the performance tests used to evaluate unmanned aircraft, compare performance results to manufacturer reported performance data, and compare different unmanned platforms.[5] One project to systematically compare different platforms was the sUAS Consumer Guide project at the Worldwide campus of Embry-Riddle Aeronautical University. This project was created for novice users and evaluated 12 commercially off-the-shelf (COTS) multirotor aircraft. These systems were graded on several criteria including cost, ease of operation, performance, and accuracy of advertised capabilities.[5,31] Nevertheless, such testing like the sUAS Consumer Guide is inherently limited to only the included platforms and the specific application criteria set for testing. Therefore, the evaluation of suitability for a new application would require the setup of an entire new test series specific to the intended application purposes. Furthermore, a prediction of performance enhancements through custom configurations and modifications would still be limited.

One motivation for the current research was to broaden the scope of the sUAS Consumer Guide by providing more specific performance information. The first area of focus is the static performance of the propellers and motors for these small Unmanned Aerial Vehicles (UAVs). For multirotor UAVs, the static performance directly relates to the hover capabilities and can be used to predict the hover endurance of the aircraft. By knowing the thrust and power from the propellers along with the power consumption of the electric motors, the amount of time a UAV can stay airborne can be calculated based on the available battery capacity. The propellers and motors used by the aircraft in the sUAS Consumer Guide were tested in static conditions and the propeller thrust, propeller power, motor input voltage, and motor input current were measured. This research paper presents the results of four of the aircraft. Besides testing the propellers supplied with these aircraft, a few third-party propellers that are designed for multirotor aircraft were also tested. A total of ten propeller pairs (both tractor and pusher versions) and four motors were tested.

The results of the static performance tests have several uses. The first use is that the results can be used to verify the endurance time of the aircraft listed by the manufacturer. Another use of the static data is to start building a database of performance for propellers used on small multirotor UAVs. Many propellers used with small fixed-wing UAVs have been tested,[18,19,29,32–40] but no systematic tests have been performed on the propellers used on multirotor systems. A database of performance results will provide those who design new UAVs or modify existing models some of the important information necessary to predict the performance of the new aircraft.

Lastly, another use of the database is that it provides practically relevant sets of performance data that can be incorporated into the simulation and modeling of sUAS multirotor operations. Such simulation models are currently employed in novel training and education approaches that aim to provide hands-on learning experiences through computer-mediated environments. For example, at Embry-Riddle Aeronautical University's Worldwide Campus, an Aerial Robotic Virtual Lab (ARVL) is currently employed in a variety of online, distributed courses to allow student exploration of physical relationships concerning different aspects of sUAS such as configuration, flight and mission planning, and sensor application.[41] Through interactive labs, students can explore system operation and component function and take physical measurements in a simulated environment. Incorporation of real-world testing data such as the research presented in this paper will enable a higher fidelity of these simulation approaches both in absolute (i.e., the degree of user perceived realism) and relative perceptivity (i.e., the degree of real-world-comparable user behavioral response to the simulation[42]), and it can, thus, increase task- and objective-specific usefulness and usability of the virtualization.[43,44] Such virtual lab approaches in education have demonstrated the potential to provide a meaningful distant application of hands-on activities in STEM education[45] and may allow the design of more authentic course assignments and assessments.

II. Propulsion Systems Tested

Static performance results from ten propeller pairs and four motors are presented in this paper. The list of the propellers, the motor used with each propeller, the propeller diameters, and the voltage used

to power the motors is given in Table 1. The diameter values provided are the true diameters that were measured to the nearest 0.05 in. The voltage used was based on the rated voltage of the battery used for the aircraft model. Each propeller listed was a propeller pair consisting of a tractor and pusher propeller. The tractor and pusher nomenclature is used in this paper based on how the propeller manufacturers, such as APC and Master Airscrew, distinguish their propellers. There is an inconsistency with the small UAV manufacturers in the naming convention of the propellers. The tractor and pusher nomenclature is used with some while other companies will use counter-clockwise and clockwise. The use of right-handed and left-handed has also been noted. For the propellers tested in this paper, a tractor propeller is right-handed and spins counter-clockwise when viewed from the front of the propeller. A pusher propeller is left-handed and spins clockwise when viewed from the front of the propeller.

Table 1: Aircraft Motors and Propellers

Aircraft Motor	Propeller	Diameter (in)	Voltage (V)
3D Robotics Solo	Solo	10.0	14.8
	APC 10×4.5 MR	10.0	14.8
DJI Phantom 3	DJI 9450 Plastic	9.45	15.2
	DJI 9450 Carbon	9.45	15.2
	APC 9.5×5 MR	9.5	15.2
	Master Airscrew MR 9.4×5	9.45	15.2
	APC 9×4.5 MR	9.0	15.2
	Master Airscrew MR 9×4.5	9.05	15.2
Hubsan X4 Pro	X4 Pro	9.4	11.1
Helimax FORM500	FORM500	12.05	11.1

A. Motors

Pictures of the four motors used for the static performance tests are shown in Figs. 1–4. The purpose of this research was not to characterize the motors nor validate any manufacturer provided motor specifications. The voltage and current input to the motors were measured to calculate the power consumption of the motor and propeller system. The amount of power drawn by the motor directly relates to the allowable time in flight for these multirotor systems. While not used for this research, the manufacturers of the Solo and FORM500 did provide the motor velocity constant for their respective motors. The 3D Robotics Solo motor has a value of 880 K_v found from their website,[46] and the Helimax FORM500 has a value of 800 K_v written on the motor casing.

The voltage and current were measured before the electronic speed controller (ESC). The ESC for the FORM500 was available for purchase as a standalone component and was used with the FORM500 motor. Since the respective ESCs for the Solo, X4 Pro, and Phantom 3 were not available for purchase as a standalone component, a Castle Creations DMR 30/40 ESC was used for these motors.

B. Propellers

The chord and twist distribution for each propeller was measured using the PropellerScanner software created by Hepperle.[47] With this software, pictures of the front and side of the propeller are used to determine the chord and twist distributions. Uhlig, et al.[34,48] showed that the PropellerScanner software provided an accurate measure of the chord distribution but can underestimate the twist angles. While the twist measurement from PropellerScanner might not be as accurate as physically measuring the angle, the software does provide an easy way to compare the geometries of different propellers. Figures 5–14 show the chord and twist distribution of each propeller pair tested. Also included is a picture of the front and side view of the propellers.

As shown in Table 1, some APC and Master Airscrew propellers were also tested. The APC 10×4.5 MR propeller is marketed as a replacement propeller for the Solo. Both the APC 9.5×5 MR and Master

Figure 1: Motor for the 3D Robotics Solo.

Figure 2: Motor for the DJI Phantom 3.

Figure 3: Motor for the Hubsan X4 Pro.

Figure 4: Motor for the Helimax FORM500.

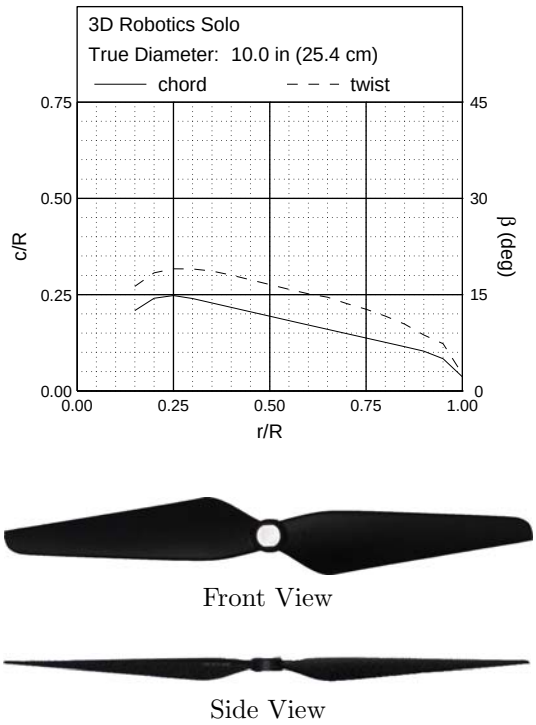

Figure 5: Chord and twist distribution for the 3D Robotics Solo propeller.

Airscrew MR 9.4×5 are marketed as replacement propellers for the DJI Phantom 3. The APC 9×4.5 MR and the Master Airscrew MR 9×4.5 are not for any specific aircraft but are part of both companies' multirotor

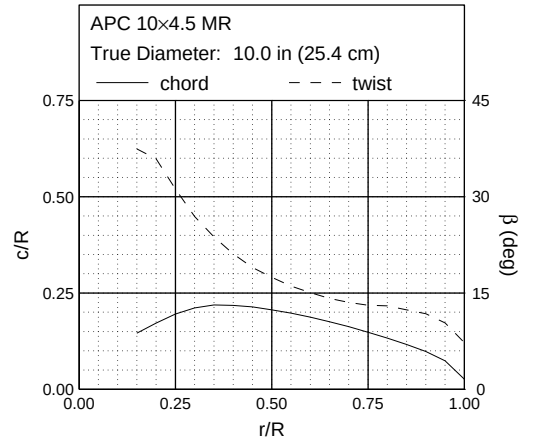

Front View

Side View

Figure 6: Chord and twist distribution for the APC 10×4.5 MR.

propeller series. A comparison between the standard Solo propeller and the APC 10×4.5 MR propeller is given in Fig. 15. The chord distribution is similar on the outer part of the blade, but the Solo propeller is larger near the hub while the APC propeller is a little larger near the middle of the blade. Both propellers have the same angle at the 75% location, so they have the same pitch.

Figure 16 shows the comparison between the two versions of the DJI Phantom 3 propellers. Figure 17 shows the two versions of the DJI Phantom 3 propellers and also includes the APC 9.5×5 MR and Master Airscrew MR 9.4×4 propellers, which are marketed as replacement propellers for the Phantom 3. The chord distribution of the two DJI propellers are the same, but the carbon propeller has larger twist angles than the plastic version. The APC and Master Airscrew propellers have a similar shape to their chord distributions, but the Master Airscrew propeller has a wider blade. The twist distribution is similar between the APC and Master Airscrew propellers for the inner half of the blade. For the outer 40% of the blade, the APC has a larger twist and is similar in value to the carbon version of the DJI propeller. The propeller used on the Hubsan X4 Pro has a similar shape and diameter to the DJI propellers. Figure 18 compares the DJI propellers and Hubsan propeller. The chord distribution of the Hubsan propeller is nearly identical to the DJI propellers; however, the twist distribution is not similar different. While the twist distribution is different, the Hubsan propeller does have the same pitch (angle at the 75% location) as the plastic version of the DJI propeller.

The geometry for the three multirotor APC propellers are compared in Fig. 19. Since each propeller has a different pitch-to-diameter ratio, there is an expected differnce in the pitch anglle at the 75% location. The chord distribution is nearly the same except for the inner part of the blade where the 9.5×4 propeller is wider. The pictures of the three propellers (Figs. 6, 9, and 11) show that the 9.5×4 looks different from the other two. The 9.5×4 also has swept tips but this difference does not appear in the chord distribution. While other APC propeller types have been tested with this setup,[18,19,32,33,35,49] the APC MR propellers have not. To see how the MR propellers differ in shape from other APC propellers, the 9×4.5 MR was compared to a Slow Flyer[32,33,35] (Fig. 20) and Thin Electric[32,33,35] (Fig. 21) with similar pitch-to-diameter ratios. The geometry comparison is shown in Fig. 22. The chord distributions for the MR and Thin Electric are similar except that the MR propeller is thinner from 35% to 75% along the blade. The Slow Flyer has a

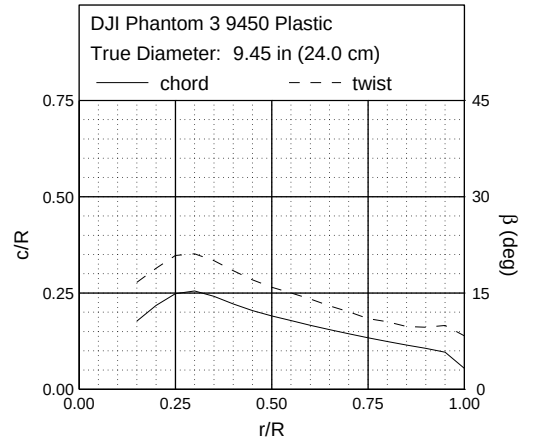

Front View

Side View

Figure 7: Chord and twist distribution for the DJI Phantom 3 9450 plastic propeller.

substantially different chord distribution. The twist distribution for the three propellers are similar except that the twist for the Slow Flyer is reduced at locations less than 35%.

The final geometry comparison shown in Fig. 23 is between the two Master Airscrew propellers: 9.4×5 and 9×4.5. The chord distribution is nearly identical and the twist distribution is similar in shape. A difference in the twist angle is seen in the outer quarter of the blade; however, the listed pitch-to-diameter ratios are different and the propeller with the larger given ratio (9.4×5) does show a larger angle at the 75% location.

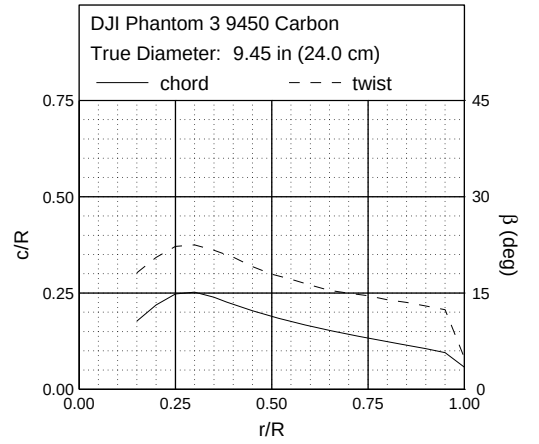

Front View

Side View

Figure 8: Chord and twist distribution for the DJI Phantom 3 9450 carbon propeller.

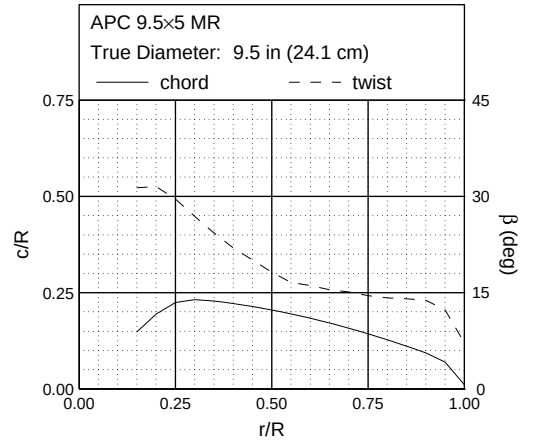

Front View

Side View

Figure 9: Chord and twist distribution for the APC 9.5×5 MR.

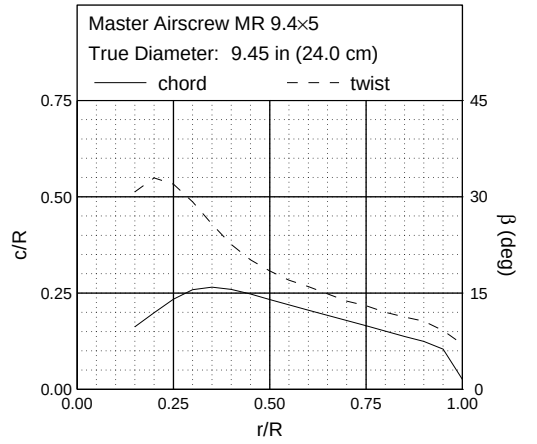

Front View

Side View

Figure 10: Chord and twist distribution for the Master Airscrew MR 9.4×5.

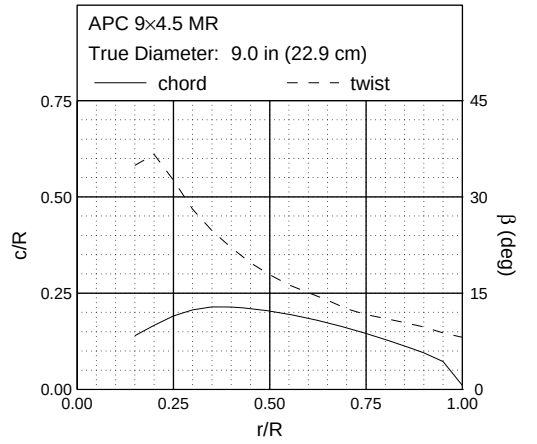

Front View

Side View

Figure 11: Chord and twist distribution for the APC 9×4.5 MR.

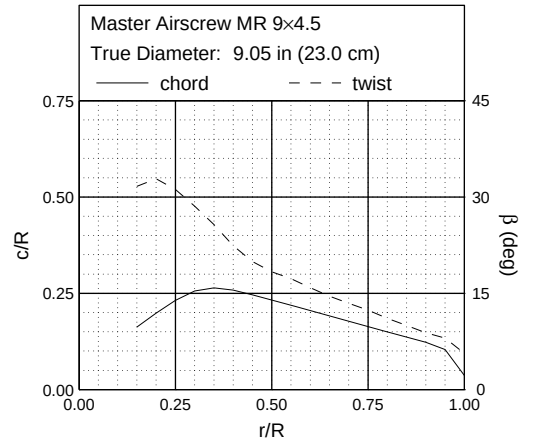

Front View

Side View

Figure 12: Chord and twist distribution for the Master Airscrew MR 9×4.5.

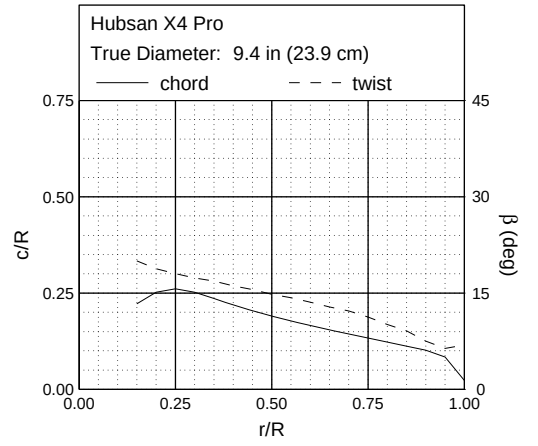

Front View

Side View

Figure 13: Chord and twist distribution for the Hubsan X4 Pro propeller.

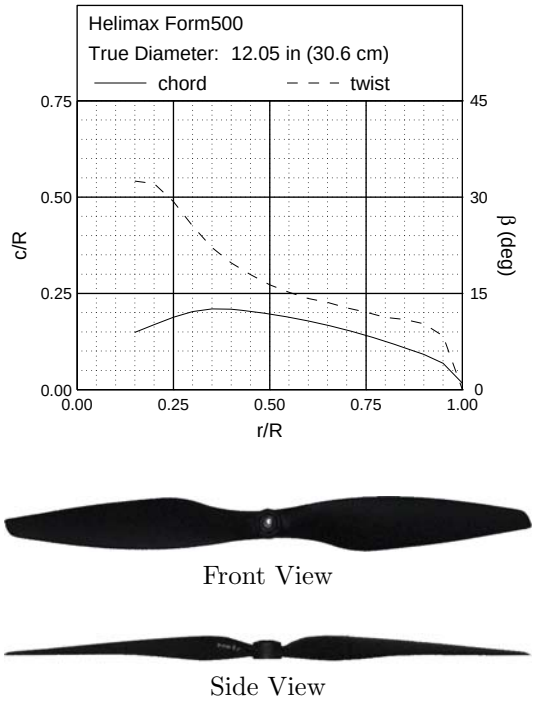

Figure 14: Chord and twist distribution for the Helimax FORM500 propeller.

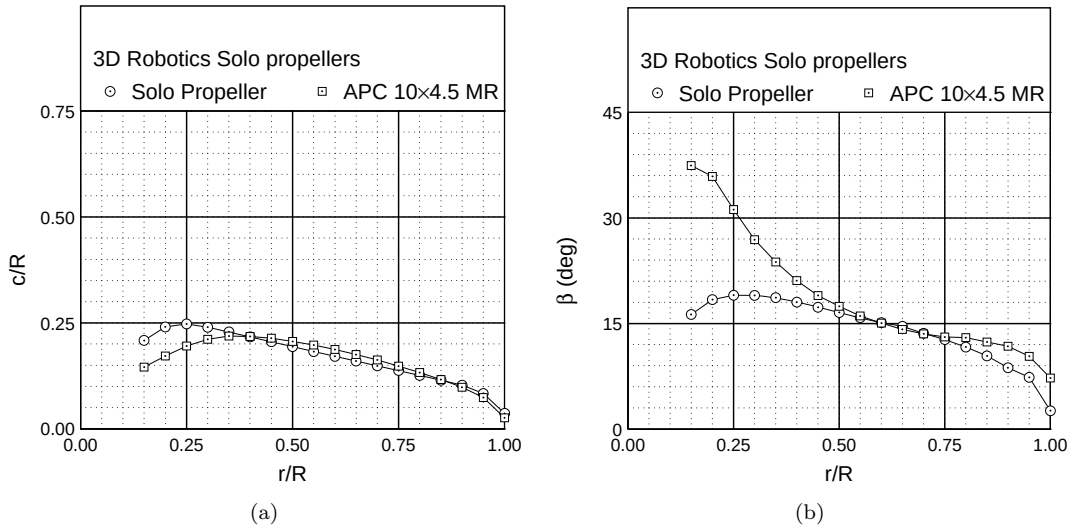

(a) (b)

Figure 15: Comparison between the standard Solo propeller and the APC 10×4.5 MR propellers: (a) chord distribution and (b) twist distribution.

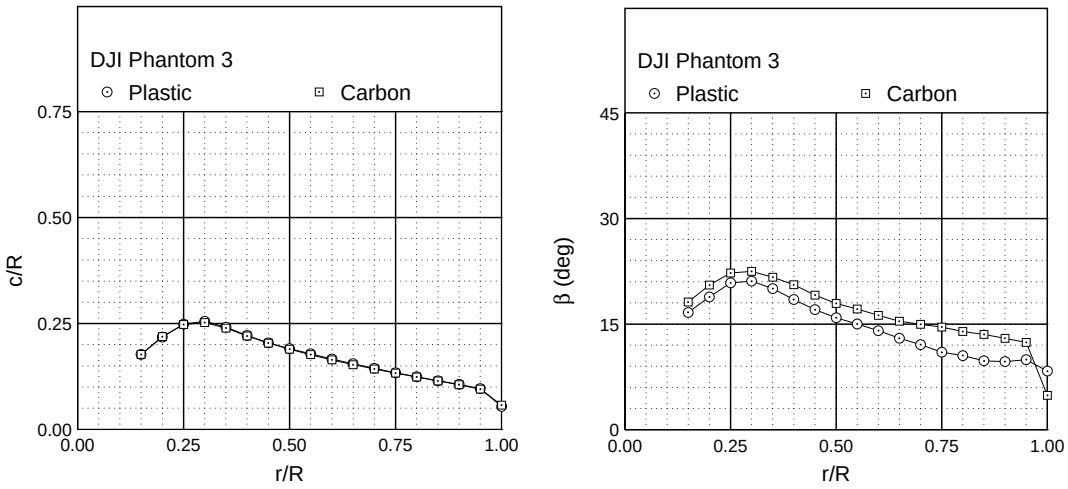

(a) (b)

Figure 16: Comparison between the DJI Phantom 3 propellers: (a) chord distribution and (b) twist distribution.

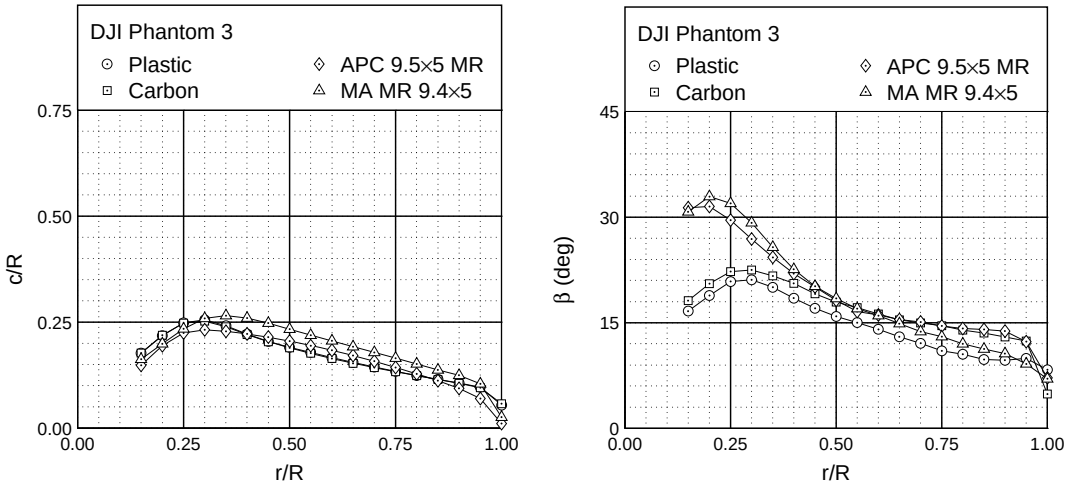

(a) (b)

Figure 17: Comparison of the DJI Phantom 3 propellers, the APC 9.5×5 MR, and the Master Airscrew MR 9.4×5: (a) chord distribution and (b) twist distribution.

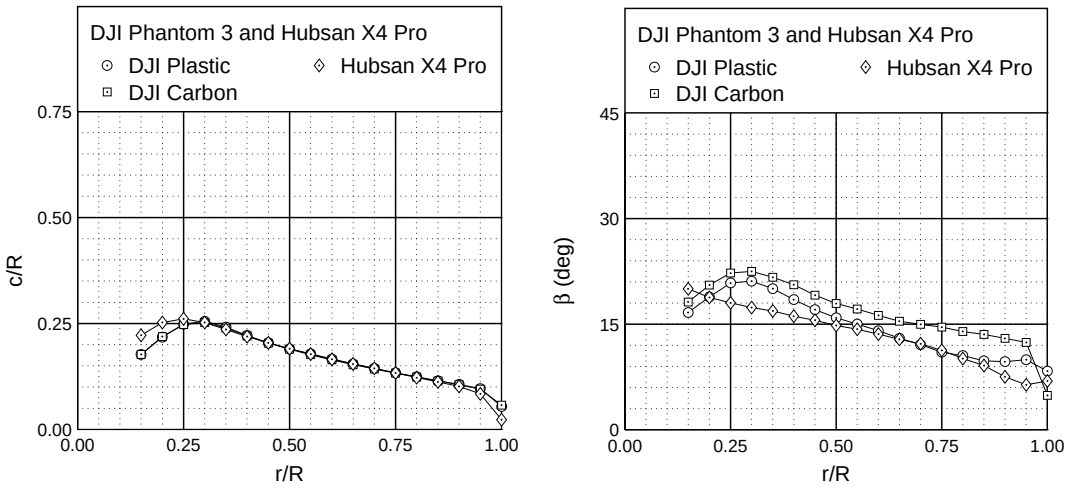

(a) (b)

Figure 18: Comparison of the propellers for the DJI Phantom 3 and the Hubsan X4 Pro: (a) chord distribution and (b) twist distribution.

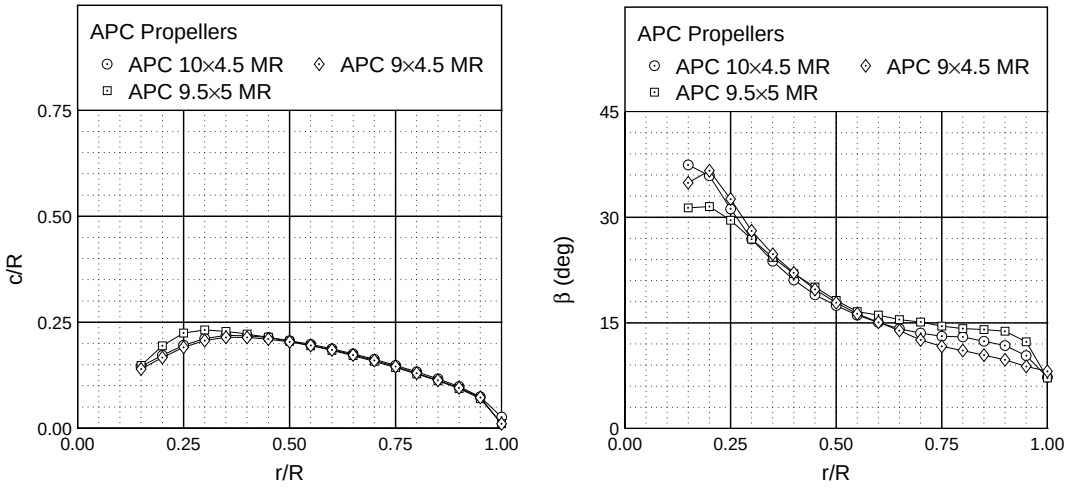

(a) (b)

Figure 19: Comparison of the multirotor APC propellers: (a) chord distribution and (b) twist distribution.

Front View

Side View

Figure 20: Front and side view of the APC 9×4.7 Slow Flyer.

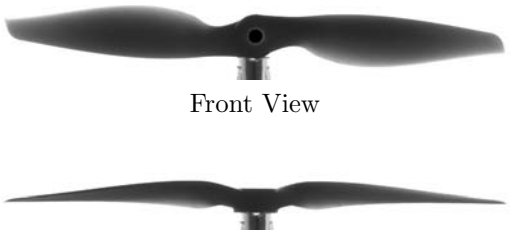

Front View

Side View

Figure 21: Front and side view of the APC 9×4.5 Thin Electric.

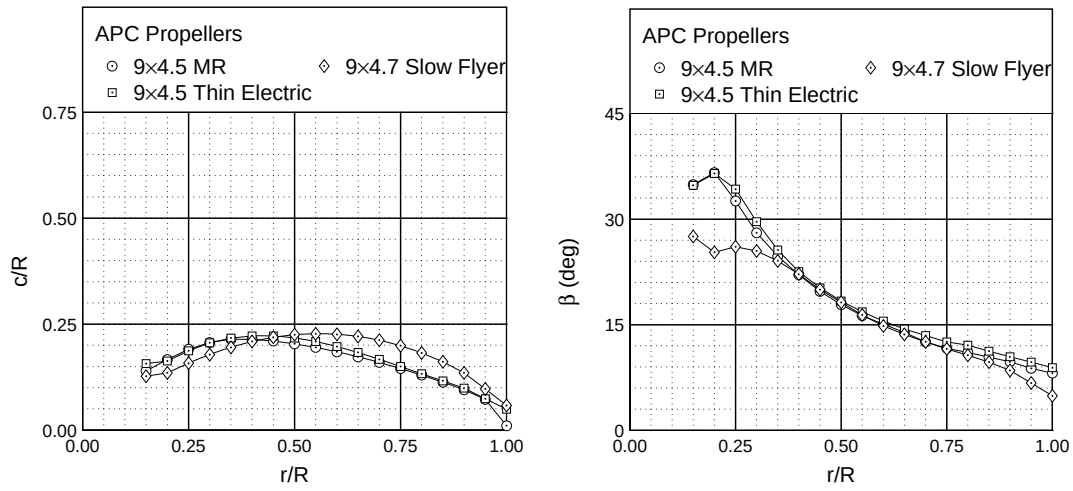

(a) (b)

Figure 22: Comparison of the APC MR, Slow Flyer, and Thin Electric propellers: (a) chord distribution and (b) twist distribution.

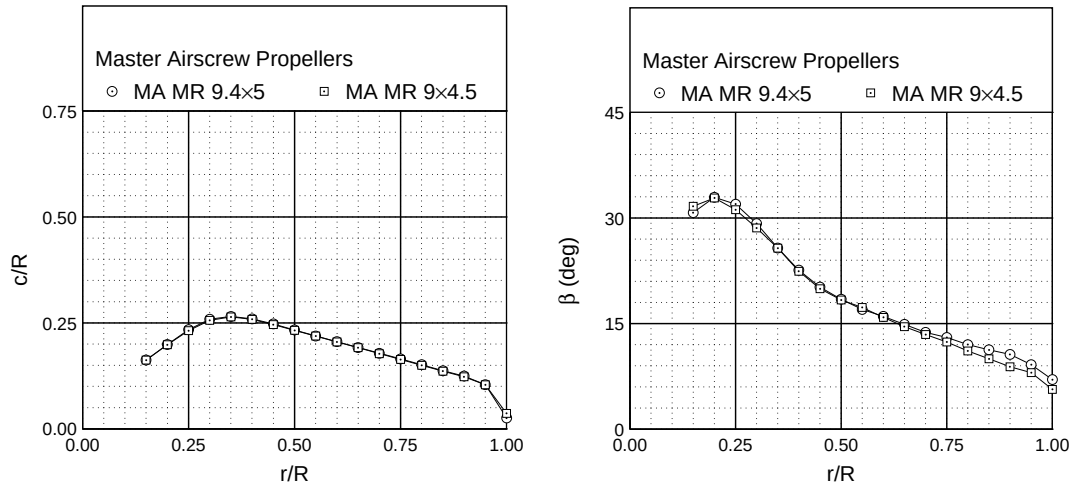

(a) (b)

Figure 23: Comparison of the Master Airscrew propellers: (a) chord distribution and (b) twist distribution.

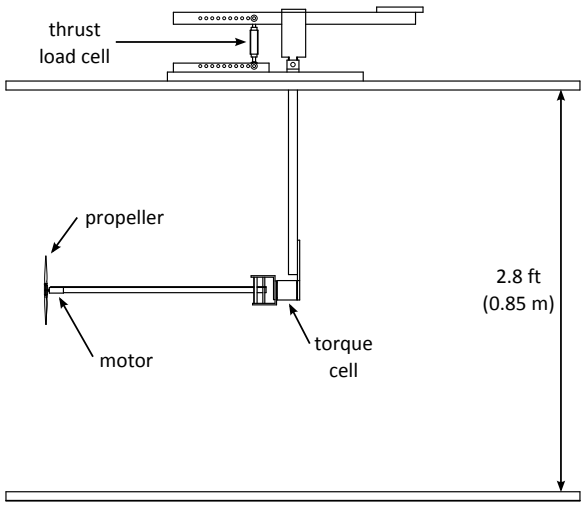

Figure 24: Propeller thrust and torque balance.

III. Experimental Methodology

A. Equipment

Propeller and motor tests were conducted in the UIUC Aerodynamics Research Laboratory (ARL) using the thrust and torque balance shown in Fig. 24 with small modifications. Since only static performance was measured for this research, the balance was set up outside of a wind tunnel. The other modification was that the torque cell was moved to a location immediately behind the motor. The torque cell was moved to decrease the moment on the torque cell produced by the weight of the motor sting. Figure 24 shows the original torque cell location and not the new location directly behind the motor.

Thrust was measured using the T-shaped pendulum balance that pivoted about two flexural pivots and was constrained on one side by a load cell.[32] An Interface SM S-Type load cell with a load capacity of 25 lb (111 N) was used for these tests. The balance was designed to allow the load cell to be placed in ten different locations to use the full range of the load cell based on the thrust produced. The load cell locations ranged from 3.25 in (8.26 cm) from the pivot point to 7.75 in (19.69 cm) in 0.5-in (1.27-cm) increments.

The torque from the propeller was measured using a reaction torque sensor (RTS) from Transducer Techniques. A 100 oz-in (0.706 N-m) transducer was used. The torque cell was placed between the motor and the motor sting. To remove as much of the testing rig from the propeller slipstream as possible, a fairing was used to surround the motor sting, balance support arm, and wires. Additional details about the balance and fairing can be found in Deters, et al.[18,19]

A red laser and phototransistor were used to measure the propeller RPM. As the propeller spins, the propeller blades block the laser and cause the voltage read from the phototransistor to drop near zero. The peaks from the resulting square wave were counted over a sample time to determine the RPM. Specifications about the RPM measurement system are available in Deters et al.[18,19]

To provide power to the motors, a BK Precision 1688B power supply was used. This power supply has the capability to be connected to a personal computer through a Universal Serial Bus (USB) cable and have the voltage and current recorded. The voltage from the power supply was also measured by a TekPower TP8236 USB Digital Multimeter and recorded by the computer. The current from the power supply was not measured by a second multimeter due to the 10 A limitation on the multimeter. The ambient pressure was measured using a Setra Model 270 pressure transducer, and the ambient temperature was measured using a digital thermometer.

B. Testing Procedure

During a static performance test, the thrust, torque, input voltage, and input current were measured over a range of RPMs. A LabVIEW® program was written to automatically set the propeller RPM and record the resulting performance data. To control the RPM, a personal computer commanded a voltage to a modified

ServoXciter EF from Vexa Control using a National Instruments PCI-6031E 16-bit analog-to-digital data acquisition (DAQ) board. The ServoXciter then sent a signal to the electronic speed controller to rotate the motor. Once the desired RPM value was reached, the thrust and torque data were recorded by the DAQ board. Simultaneously with the thrust and torque measurements, the ambient pressure was also measured. To fully capture the RPM, the voltages from the phototransistor were recorded at a higher rate than the rest of the measurements. The propeller RPM was measured first followed by the measurement of the thrust and torque. The LabVIEW program measured the voltage and current from the power supply and the voltage reading from the multimeter after the thrust and torque measurements.

C. Calibration

Since the DAQ board only records voltages from the torque transducer and load cell, each voltage is converted to a physical measurement through calibration curves. Thrust calibration used precisely measured weights and a low-friction pulley system to create an applied axial load to simulate thrust on the load cell. By increasing and decreasing a known force on the load cell, a linear relationship between the thrust and voltage was determined. For torque calibration, the precision weights were used with a known moment arm to create a torque, and by adding and removing weights, a linear relationship between the torque and voltage was calculated. These calibration procedures were performed regularly to ensure consistent results, and any change in the slopes were typically 1% or less.

D. Data Reduction

Using the measured ambient pressure and temperature, the air density was calculated from the equation of state

$$p = \rho R T \tag{1}$$

where R is the universal gas constant. The standard value of 1716 $\text{ft}^2/\text{s}^2/^\circ\text{R}$ (287.0 $\text{m}^2/\text{s}^2/\text{K}$) for air was used.

Propeller power is calculated from the measured propeller torque by

$$P = 2\pi n Q \tag{2}$$

Performance of a propeller is typically given in terms of the thrust and power coefficients, defined as

$$C_T = \frac{T}{\rho n^2 D^4} \tag{3}$$

$$C_P = \frac{P}{\rho n^3 D^5} \tag{4}$$

where nD can be considered the reference velocity and D^2 can be considered the reference area.

The Reynolds number of the propeller is calculated based on the rotational speed and chord at the 75% blade station. The Reynolds number is defined as

$$Re = \frac{\rho V c}{\mu} \tag{5}$$

where the viscosity μ was calculated from Sutherland's formula.

E. Verification of Static Performance Tests

To ensure that the performance data gathered during this research was accurate, a repeatability test was performed using a propeller that had been tested before. The propeller used for this test was the APC 9×4 Free Flight,[18,19] and the results are shown in Fig. 25. The results from year 2013 had the balance set up in a wind tunnel using the original torque cell and motor sting configuration as shown in Fig. 24. The motor used during the 2013 test was an AstroFlight 803P Astro 020 Planetary System with a 4.4:1 gear ratio. The current 2017 results were taken with the modified balance using the DJI Phantom 3 motor. The results from the two validation tests agreed well.

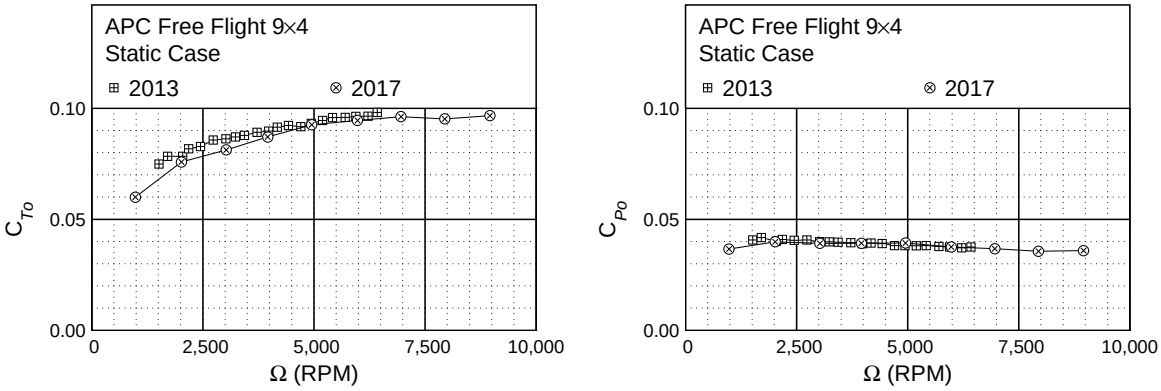

(a) (b)

Figure 25: Repeatability of the static performance of the APC 9×4 Free Flight: (a) thrust coefficient and (b) power coefficient.

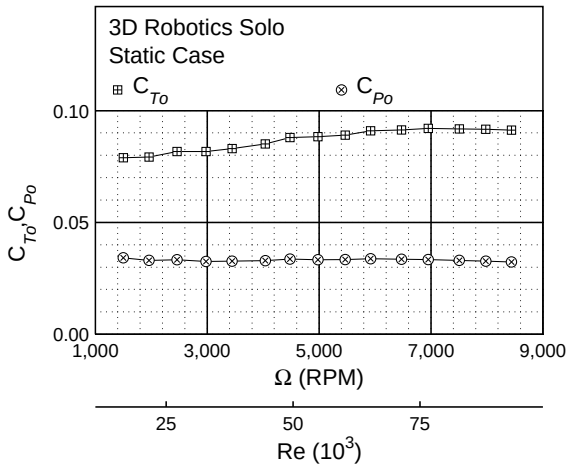

Figure 26: 3D Robotics Solo tractor propeller static performance.

IV. Performance Testing Results

A. Propeller Results

The static performance results for the ten propeller pairs are provided in this section. The order of the propeller results follows Table 1 and is based on the motor used during testing. For each propeller pair, the results of the tractor propeller are first provided, and then a comparison between the tractor and pusher propellers is shown. For the most part, the results of the tractor and pusher versions of each propeller agreed well as would be expected.

Figures 26 and 27 show the results for the propellers provided with the 3D Robotics Solo. The results for the APC 10×4.5 MR propellers sold as replacement propellers for the Solo are given in Figs. 28 and 29. The two sets of propellers for the Solo were compared, and the results are shown in Fig. 30. Both propellers show an increase in C_{T_0} with increasing RPM with the APC propeller having a larger C_{T_0} at all RPM values. The APC propeller also has a larger C_{P_0} for all RPM values.

Both versions (plastic and carbon) of the DJI brand propellers for the Phantom 3 were tested. The results for the plastic version are found in Figs. 31 and 32. Figures 33 and 34 show the results for the carbon version. The comparison between the two DJI brand propellers is found in Fig. 40, and the figure shows that the carbon version clearly has a larger C_{T_0} and C_{P_0} at all RPM values. The larger thrust and power

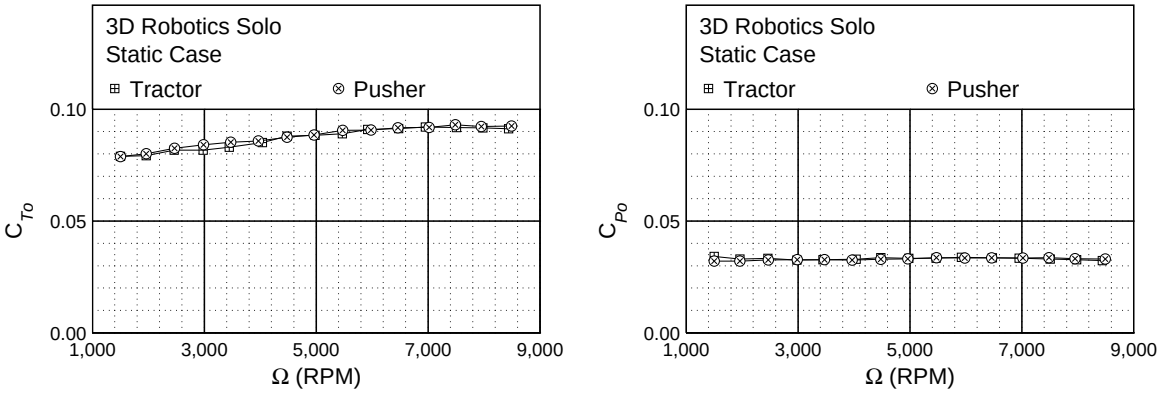

(a) (b)

Figure 27: Static performance comparison between the tractor and pusher propellers of the 3D Robotics Solo: (a) thrust coefficient and (b) power coefficient.

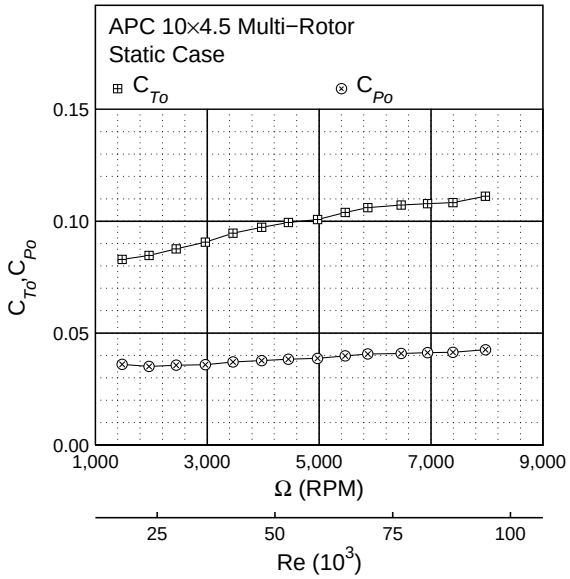

Figure 28: APC 10×4.5 MR static performance.

coefficients for the carbon version are not unexpected as the twist angles were larger for the carbon version as shown in Fig. 16.

The results for the APC 9.5×5 MR replacement propellers for the DJI Phantom 3 are shown in Figs. 36 and 37, and the results for the Master Airscrew MR 9.4×5 replacement propellers are given in Figs. 38 and 39. Figure 40 shows the comparison of the two versions of the DJI brand propellers, the APC 9.5×5 MR, and the Master Airscrew MR 9.4×5. The Master Airscrew propeller has the largest thrust coefficient but also the largest power coefficient, and the plastic DJI propeller has the lowest thrust coefficient and power coefficient. The C_{T_0} values for the carbon and APC propellers are close, but the APC propeller has a smaller C_{P_0} at lower RPM values.

Two other propellers were tested with the DJI Phantom 3 motor. While the APC 9×4.5 MR and Master Airscrew MR 9×4.5 were smaller than the propellers used with the Phantom 3, the motor provided a suitable solution to test these multirotor propellers. Results for the APC 9×4.5 MR propellers are given in Figs. 41 and 42, and results for the Master Airscrew MR 9×4.5 are shown in Figs. 43 and 44. All three APC MR propellers are compared in Fig. 45. The shape of the thrust and power coefficient curves are quite similar for

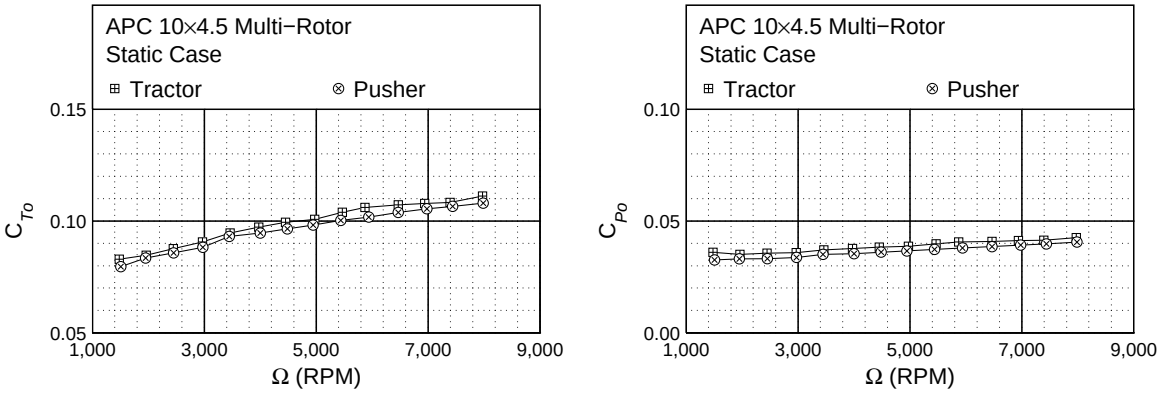

Figure 29: Static performance comparison between the tractor and pusher propellers of the APC 10×4.5 MR: (a) thrust coefficient and (b) power coefficient.

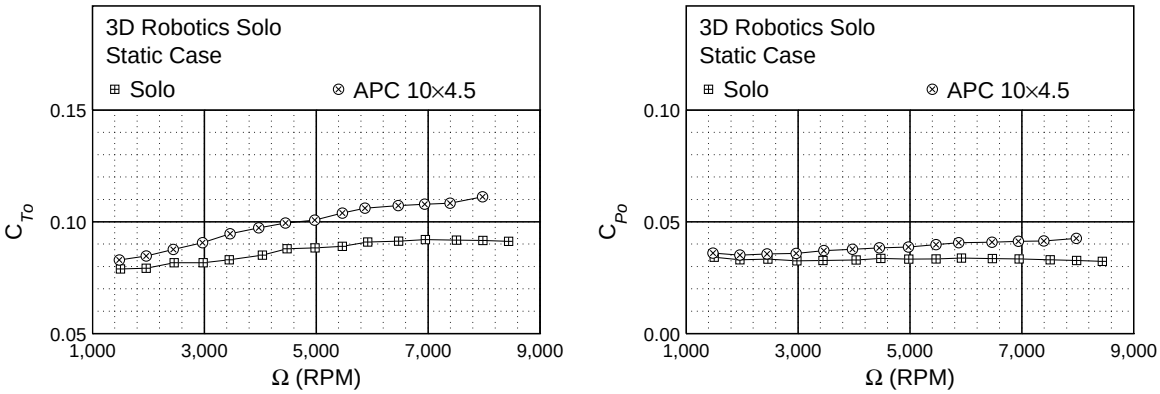

Figure 30: Static performance comparison between the Solo and APC propeller for the 3D Robotics Solo: (a) thrust coefficient and (b) power coefficient.

all three propellers. Mainly, the difference between each propeller can be explained by the pitch-to-diameter ratio. The 9.5×5 has the largest ratio and therefore the thrust and power coefficient values were the largest. The two Master Airscrew propellers were also compared with the results shown in Fig. 46. Even though the manufacturer provided pitch-to-diameter ratios were different, the thrust and power coefficient curves are nearly the same.

The static performance of the propellers for the Hubsan X4 Pro are shown in Figs. 47 and 48. The diameter of the Hubsan propeller is nearly the same as the official propellers for the DJI Phantom 3, so a comparison was made between those propellers (Fig. 49). The trend of the thrust and power coefficient curves for the Hubsan is similar to the DJI propellers. The main difference between the Hubsan and DJI propellers is that C_{T_0} and C_{P_0} are significantly less for the Hubsan propellers.

The final propeller pair presented is the Helimax FORM500. The performance results for this propeller pair are given in Figs. 50 and 51. The 12-in diameter for these propellers is the largest for the propellers presented in this research. The greatest effect of this larger diameter is the smaller RPM range during testing.

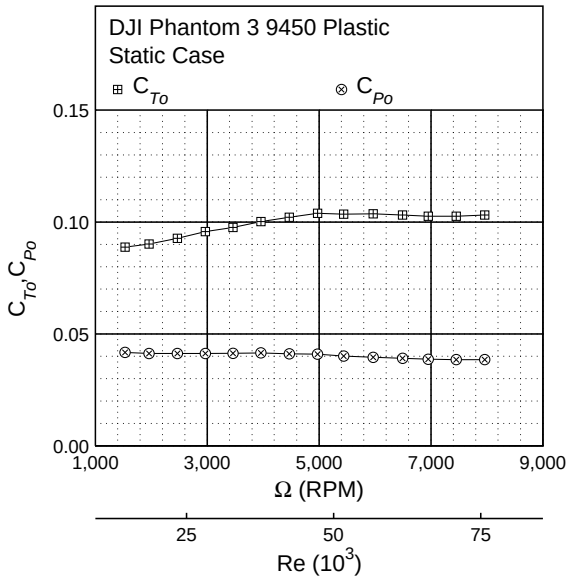

Figure 31: DJI Phantom 3 9450 plastic tractor propeller static performance.

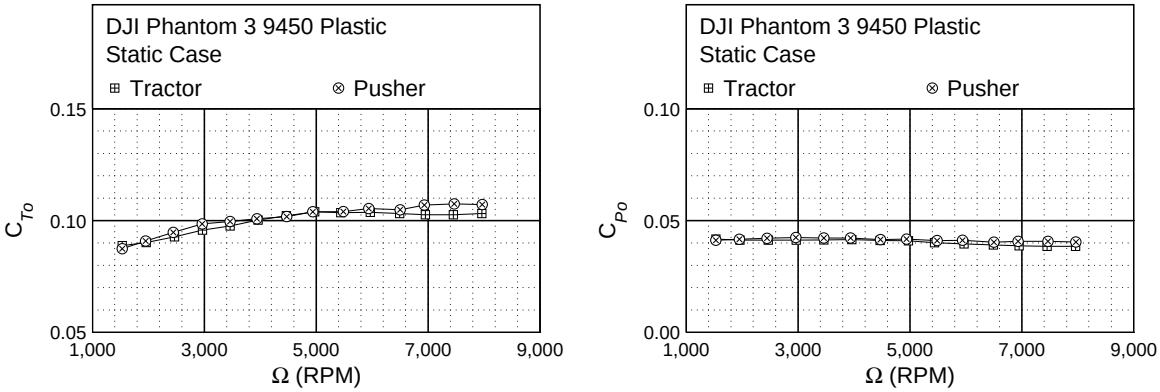

(a) (b)

Figure 32: Static performance comparison between the tractor and pusher 9450 plastic propellers of the DJI Phantom 3: (a) thrust coefficient and (b) power coefficient.

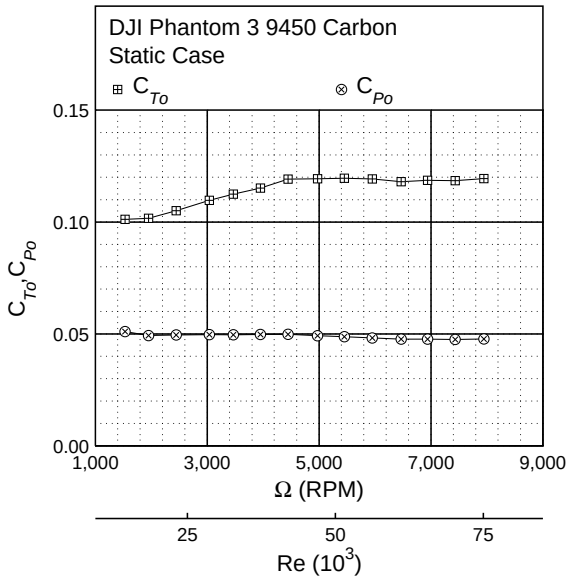

Figure 33: DJI Phantom 3 9450 carbon tractor propeller static performance.

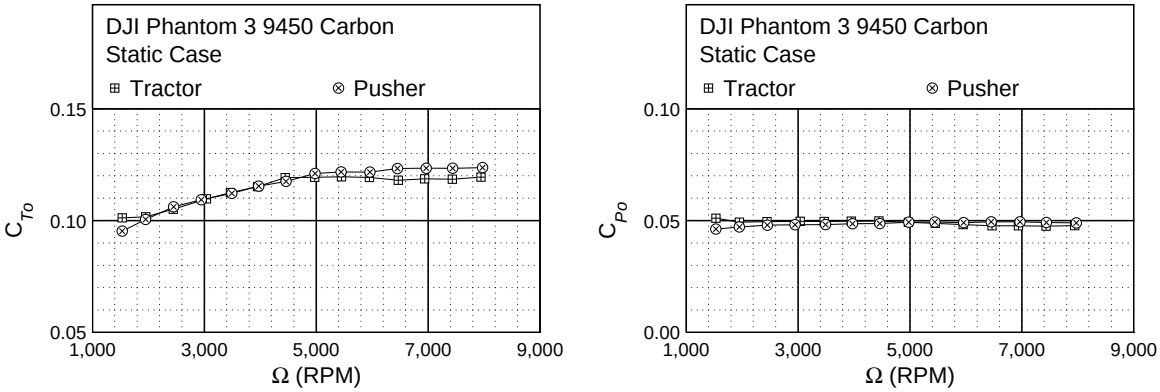

(a) (b)

Figure 34: Static performance comparison between the tractor and pusher 9450 carbon propellers of the DJI Phantom 3: (a) thrust coefficient and (b) power coefficient.

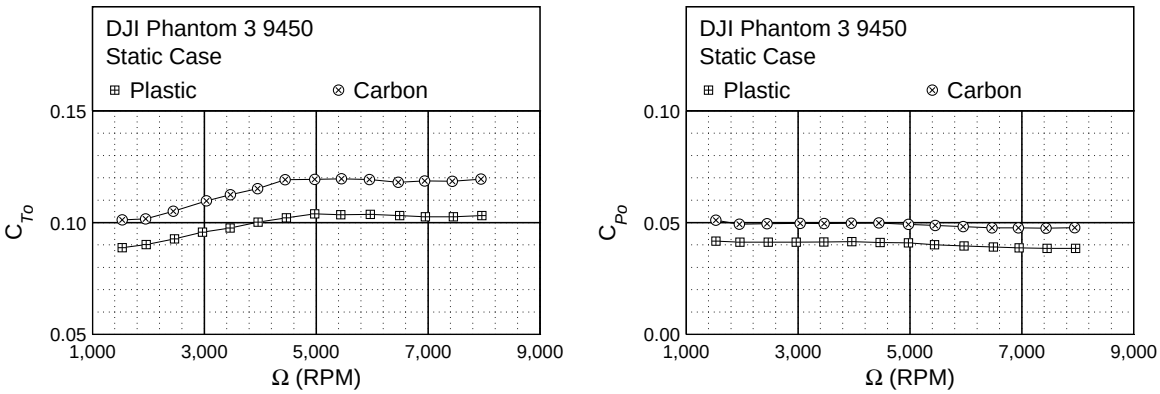

(a) (b)

Figure 35: Static performance comparison between the plastic and carbon tractor propellers of the DJI Phantom 3: (a) thrust coefficient and (b) power coefficient.

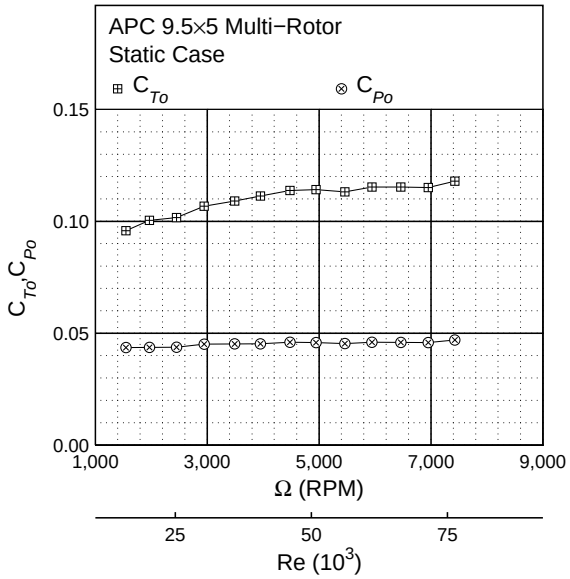

Figure 36: APC 9.5×5 MR static performance.

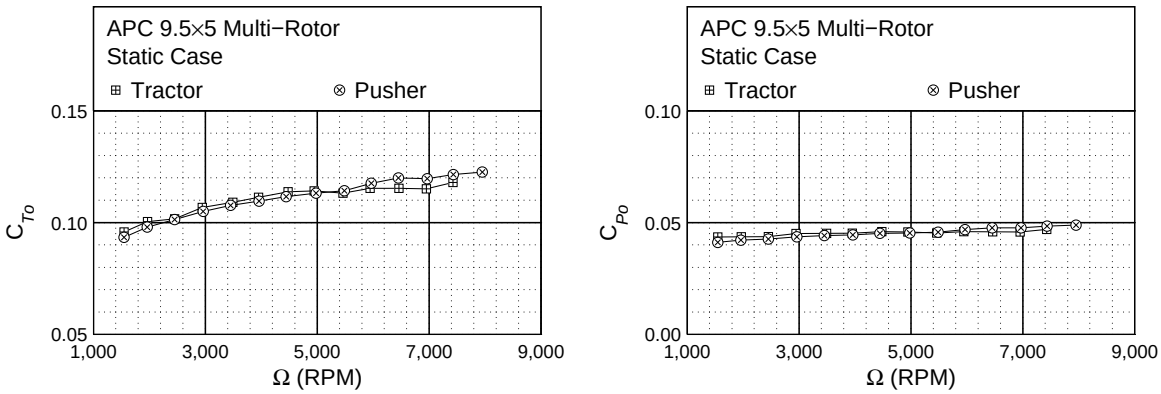

Figure 37: Static performance comparison between the tractor and pusher propellers of the APC 9.5×5 MR: (a) thrust coefficient and (b) power coefficient.

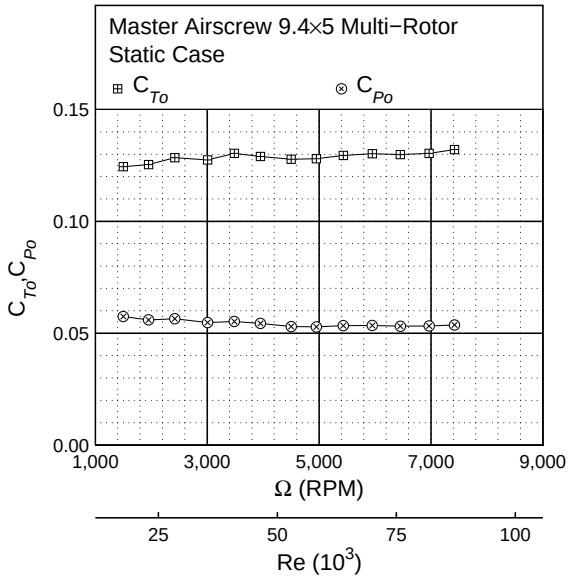

Figure 38: Master Airscrew MR 9.4×5 static performance.

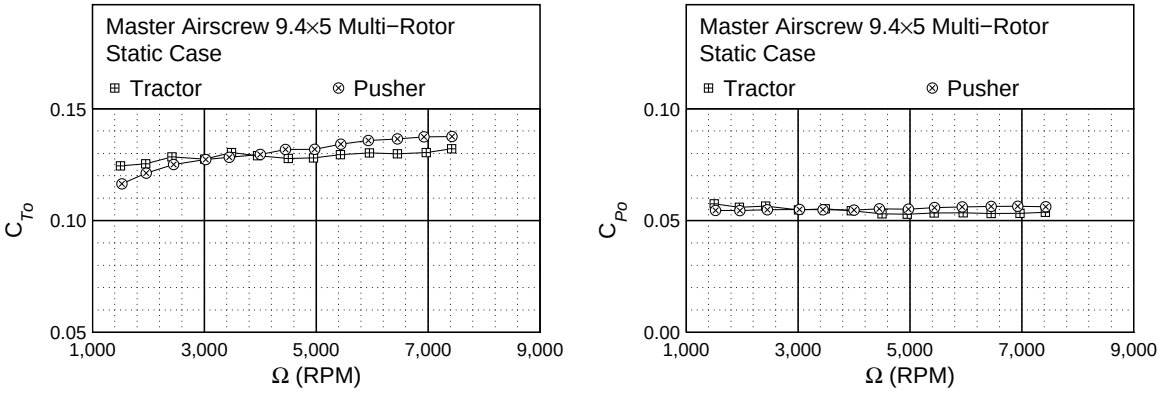

(a) (b)

Figure 39: Static performance comparison between the tractor and pusher propellers of the Master Airscrew MR 9.4×5: (a) thrust coefficient and (b) power coefficient.

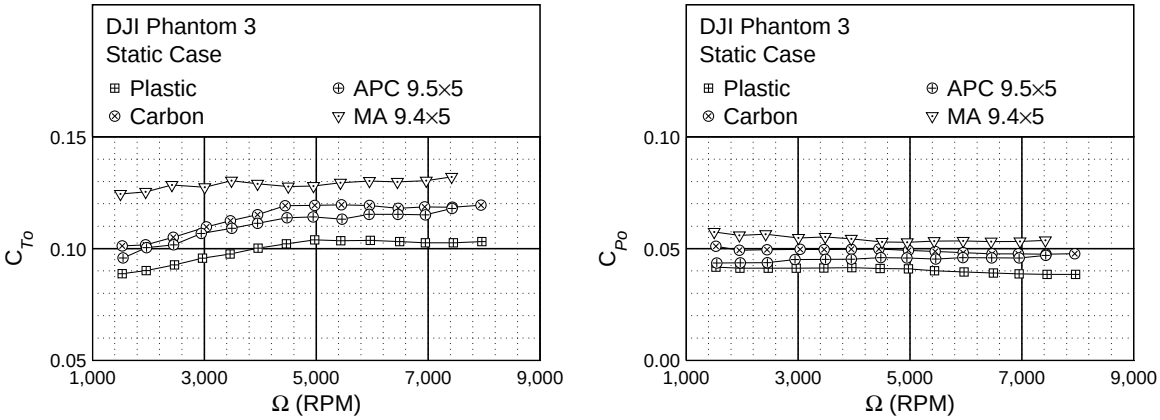

(a) (b)

Figure 40: Static performance comparison of the propellers for the DJI Phantom 3: (a) thrust coefficient and (b) power coefficient.

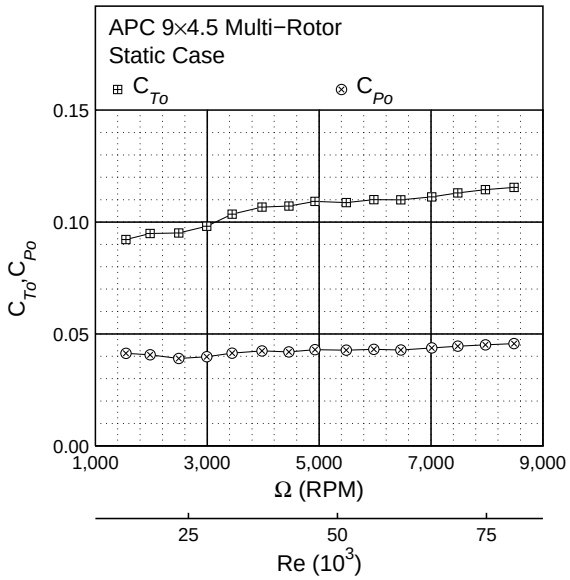

Figure 41: APC 9×4.5 MR static performance.

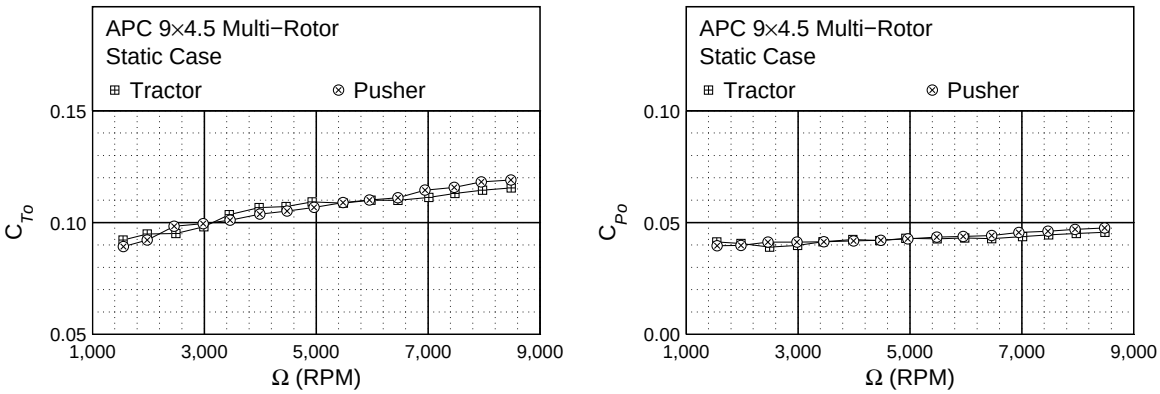

(a) (b)

Figure 42: Static performance comparison between the tractor and pusher propellers of the APC 9×4.5 MR: (a) thrust coefficient and (b) power coefficient.

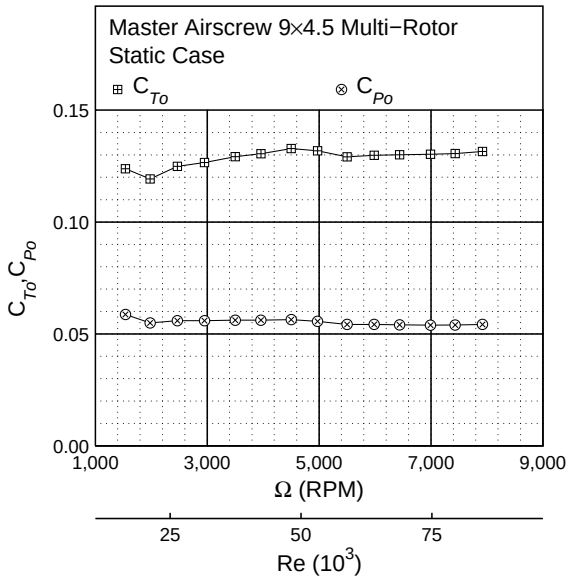

Figure 43: Master Airscrew MR 9×4.5 static performance.

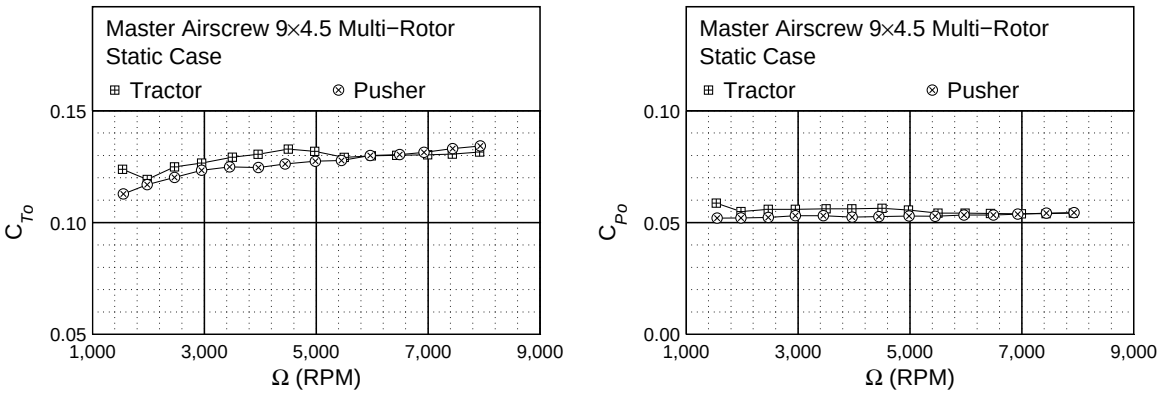

Figure 44: Static performance comparison between the tractor and pusher propellers of the Master Airscrew MR 9×4.5: (a) thrust coefficient and (b) power coefficient.

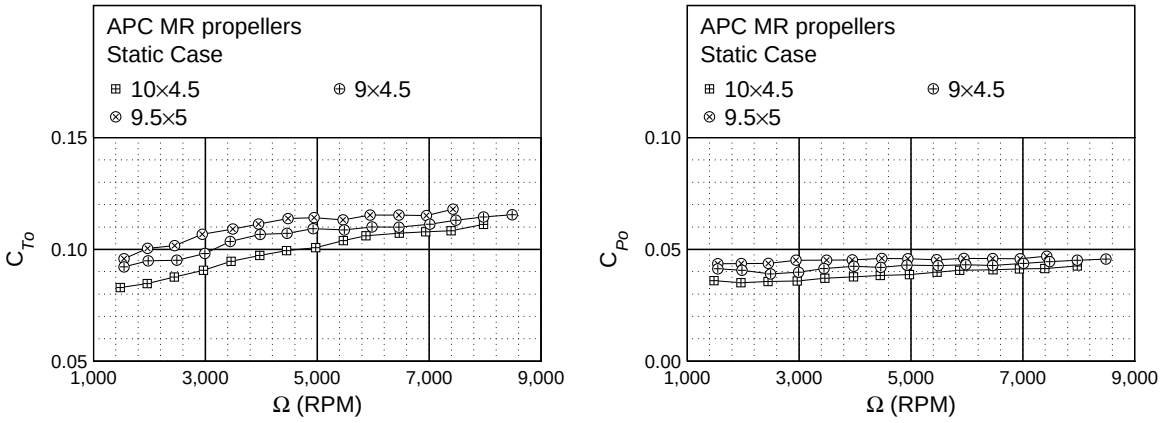

Figure 45: Static performance comparison of the APC MR propellers: (a) thrust coefficient and (b) power coefficient.

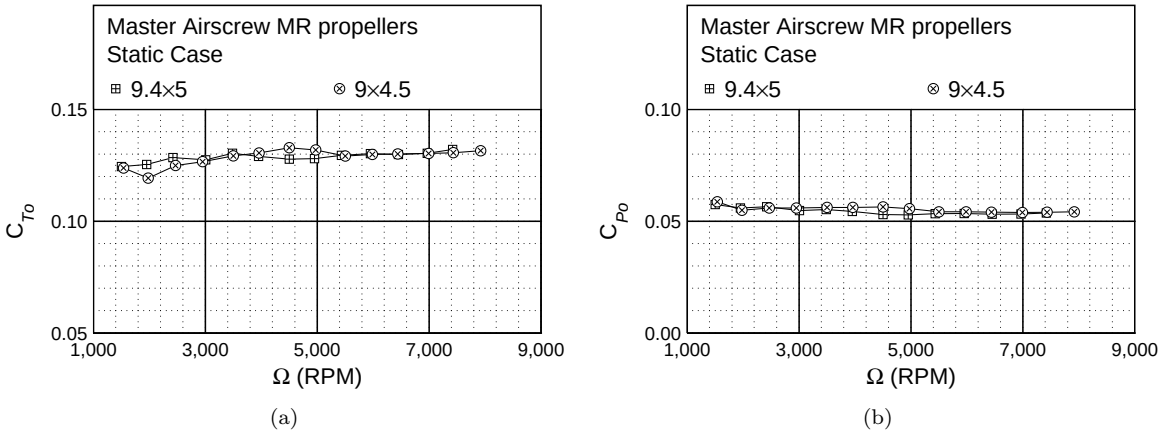

Figure 46: Static performance comparison of the Master Airscrew MR propellers: (a) thrust coefficient and (b) power coefficient.

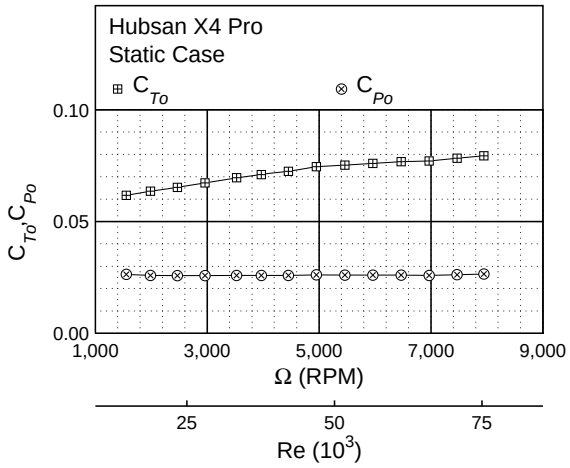

Figure 47: Hubsan X4 Pro tractor propeller static performance.

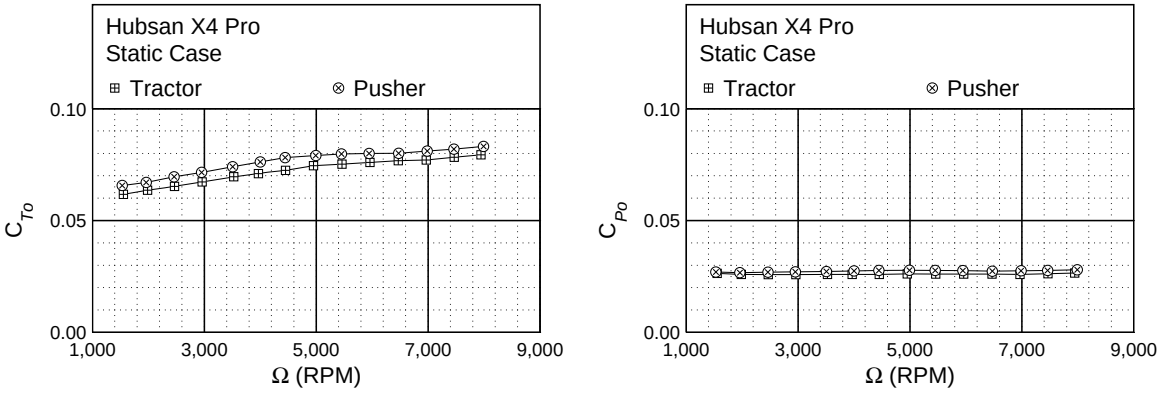

(a) (b)

Figure 48: Static performance comparison between the tractor and pusher propellers of the Hubsan X4 Pro: (a) thrust coefficient and (b) power coefficient.

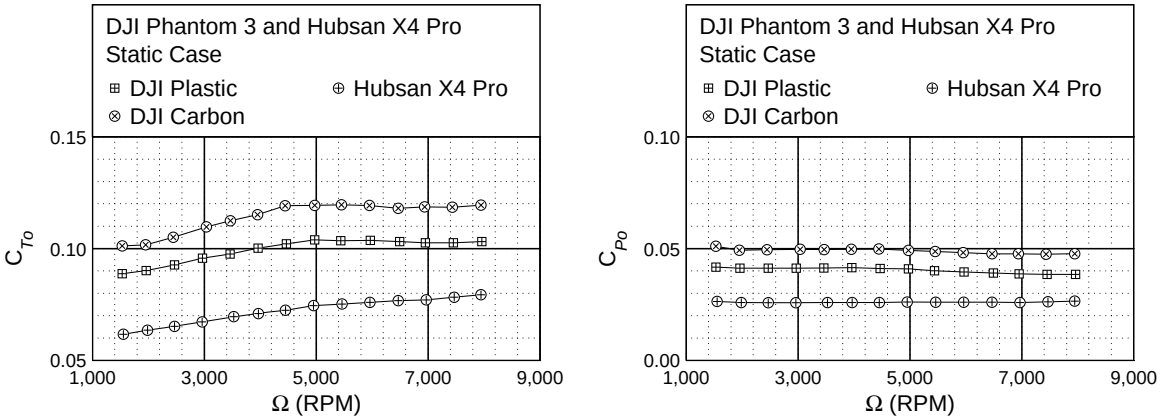

(a) (b)

Figure 49: Static performance comparison between the DJI and Hubsan propellers: (a) thrust coefficient and (b) power coefficient.

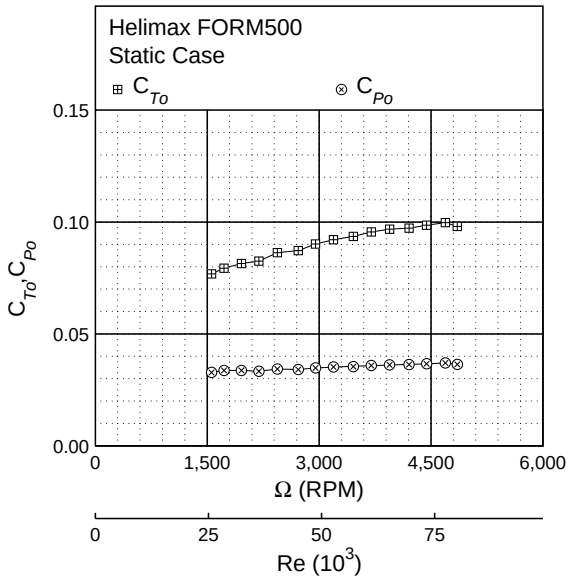

Figure 50: Helimax FORM500 tractor propeller static performance.

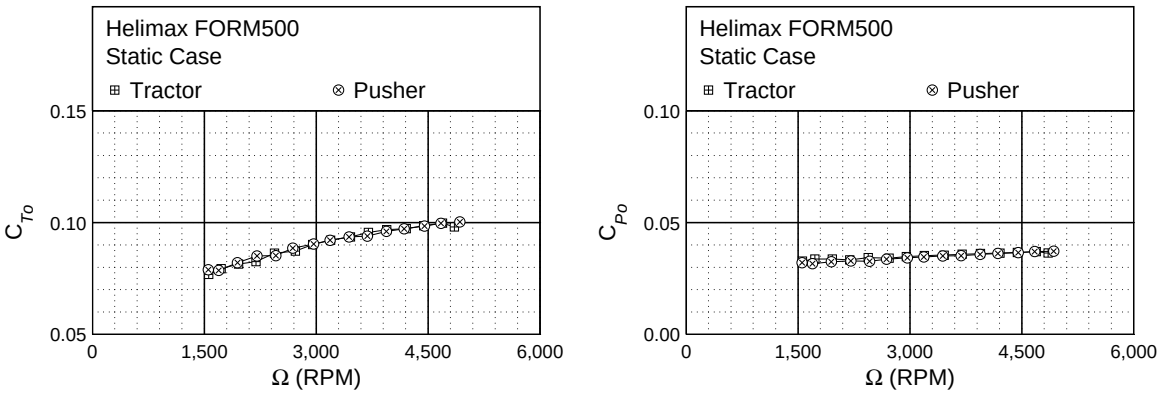

(a) (b)

Figure 51: Static performance comparison between the tractor and pusher propellers of the Helimax FORM500: (a) thrust coefficient and (b) power coefficient.

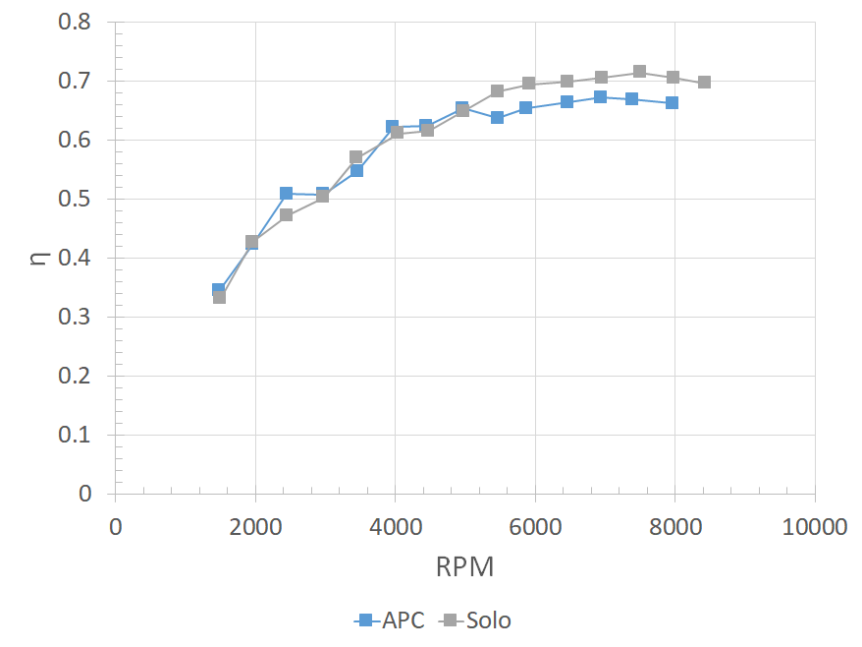

Figure 52: Motor efficiency as a function of RPM for the 3D Robotics Solo.

B. Motor Power

As mentioned before, the input motor voltage and current was measured during each test. In analyzing the results of the propeller and power measurements, one of the main questions was whether notable differences between equivalent rotor pairs for certain sUAS platforms could be established. To address this question, the electrical power input was compared with the mechanical power output measured for each propeller across the entire RPM operating range. The efficiency factor $\eta = P_{out}/P_{in}$ was plotted in relation to RPM for each of the analyzed propellers and the results visually compared. Figure 52 shows the comparison between the standard propeller found on the 3D Robotics Solo and a similar-sized designated replacement propeller, the APC 10×4.5 MR.

Notably, in the RPM range above 5000, the original Solo propeller showed a better efficiency, while at lower RPMs, efficiencies of both propellers seemed to match. To further investigate the practical implications of this noted difference, a second measure, electric current flow per thrust produced (I/T [A/lb]) was also derived from the measured data and tracked across the entire RPM range for both propellers (Fig. 53).

Similar to the differences noted in overall efficiency between the different propeller test configurations, the current per thrust ratio also indicated differences for RPMs over 5000, with the APC propeller showing a higher consumption per thrust than the standard Solo propeller. Essentially, a relationship between thrust and current flow will dictate the energy consumption rate during the hover. The required thrust will have to be equal to the weight of the vehicle while in the hover, and any associated current flow to produce this thrust, therefore, can be directly linked to the vehicle weight. For two vehicles with the same weight but different current per thrust ratios, due to different propeller choices, the rate of drain on the battery will be different, and therefore, a battery of similar capacity will be emptied in different amounts of time. Hence, the overall endurance in such hover will be different between the two configurations which has direct practical implications to the operation of the UAS.

To demonstrate this relationship in a case example, the standard 3D Robotics Solo configuration (4 lb vehicle weight equipped with a 5.2 Ah capacity battery) was applied to calculate the practical significance of the different propeller configurations. At a 4 lb vehicle weight, each of the four propellers would have to produce 1 lb of thrust, which according to the measured data equated to a required RPM of 5617 for the APC propeller. At an RPM of 5617 for the APC, the current per thrust value derived from the measurements was 4.25 A/lb, which equated to 16.98 A current flow for the entire 4-lb vehicle. At this current flow, given the standard 5.2 Ah battery, the total endurance was calculated at 18.37 min.

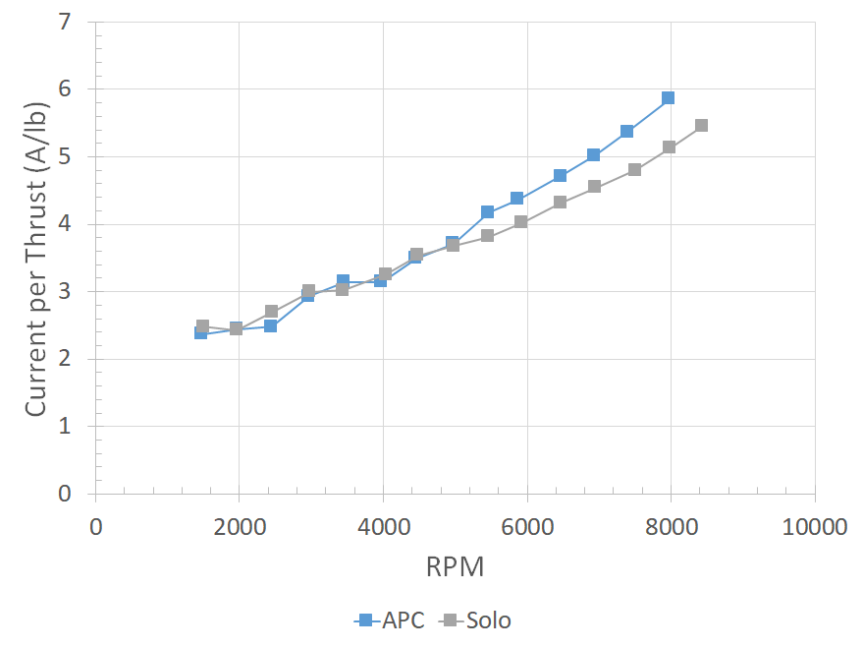

Figure 53: Current per thrust for the 3D Robotics Solo.

Similarly, 1 lb of thrust required a RPM of 6026 for the standard Solo propeller, which equated to a derived 4.06 A/lb, or a 16.25 A total current flow for the entire vehicle weight. At this consumption, total battery endurance was 19.2 min, or a 4.52% improvement over the APC configuration

A similar comparison between the DJI Phantom 3 propellers and suitable replacements is shown in Figs. 54 and 55. While the differences may not be as obvious from the plot of efficiencies in Figure 3, the current per thrust curves seem to reveal some distinctions in the upper RPM range. To build a similar case example, the performance of a typical DJI Phantom 3 (2.82 lb with a 4.48 Ah battery) platform was compared for five different propeller configurations in analogy to the previous endurance calculations. Table 2 shows the resulting theoretical total endurances for the five propeller configurations. The first four propellers in the Table are the propellers designed for the DJI Phantom 3 with diameters of about 9.45 in. The fifth propeller has a diameter of 9 in and was included to investigate any difference with using a smaller propeller. The first four propellers show very little difference in hover endurance, but the smaller propeller has an endurance that is one minute shorter. Therefore, the highest performing configuration (DJI carbon propeller) showed a total improvement of 5.44% in endurance over the lowest performing configuration (APC 9-in propeller).

Table 2: Calculated Endurance for DJI Phantom 3 Propellers

Propeller	RPM	Endurance (min)
DJI Plastic	5326	28.43
DJI Carbon	4966	28.47
APC 9.5×5 MR	5023	28.11
Master Airscrew MR 9.4×5	4790	28.38
APC 9×4.5 MR	5711	27.00

Interestingly, while the establishment of the current per thrust values was crucial for the determination of theoretical total endurance in hover, the actual plot of current per thrust curves was only telling half of the story. The higher required RPM for the APC 9×4.5 MR (Table 2 and Fig. 56) to produce sufficient thrust required a higher total current flow even though the current to thrust curve for the APC 9×4.5 MR was,

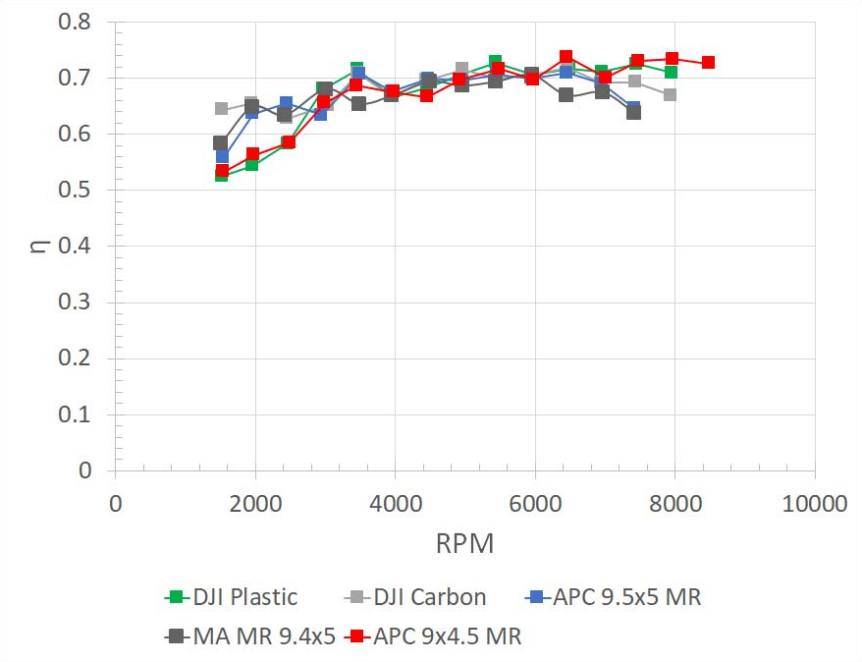

Figure 54: Motor efficiency as a function of RPM for the DJI Phantom 3.

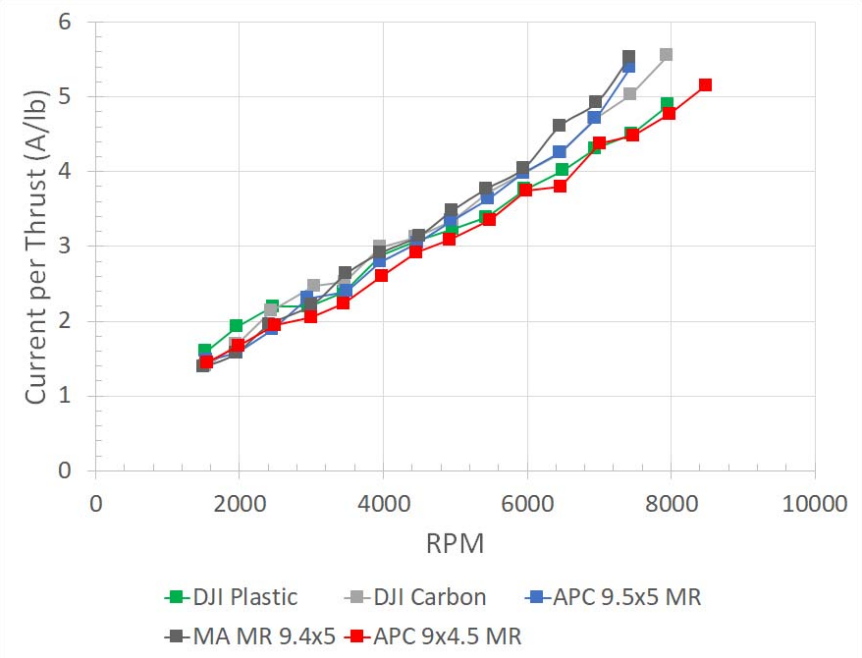

Figure 55: Current per thrust for the DJI Phantom 3.

in general, lower than the other propellers (Fig.57). Therefore, it can be concluded that further use of the derived data and associated curves has to be done always in the context of the intended operating conditions (i.e., anticipated thrust and RPM requirements) to be predictive of specific performance outcomes. A visual comparison of curves alone is insufficient.

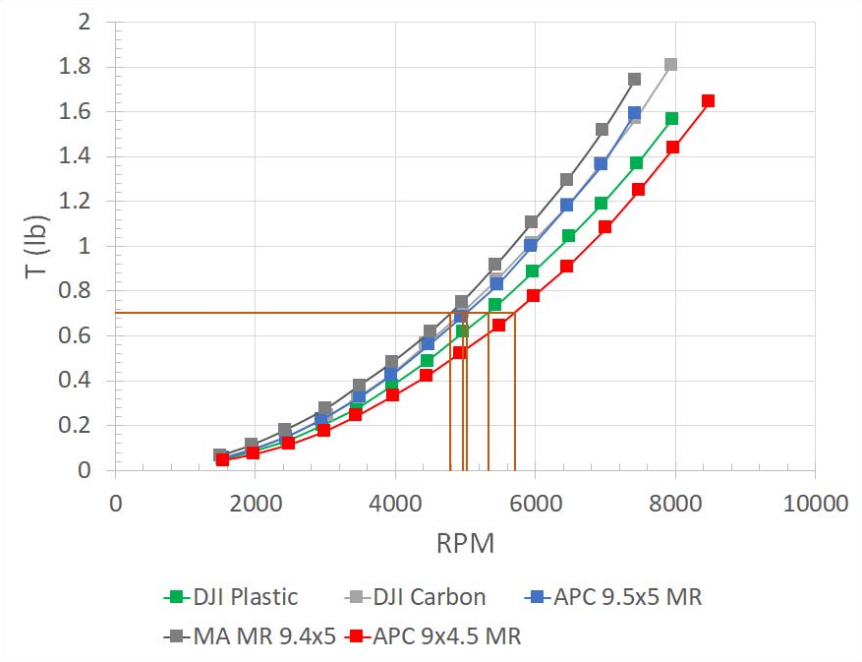

Figure 56: Thrust curves for the DJI Phantom 3.

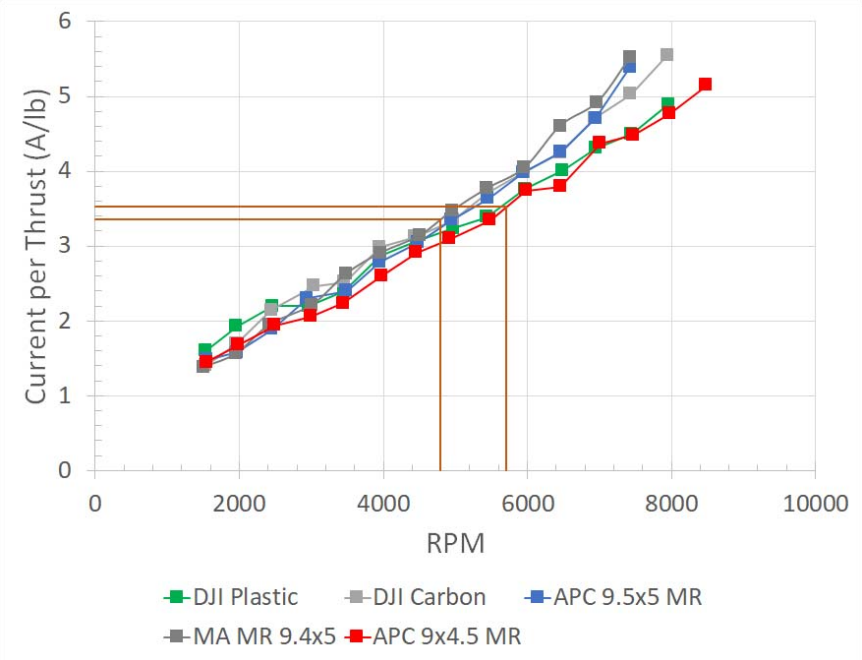

Figure 57: Current per thrust for the DJI Phantom 3 with lines at the same thrust.

V. Conclusions

To start the process of building a database of performance results of propellers used with multirotor UAVs, ten propeller pairs and four motors were tested under static conditions. The selection of the propellers and motors were based on popular COTS systems that were tested for the sUAS Consumer Guide. For this initial

set of tests, only the static performance was considered since it directly relates to the hovering capabilities of these aircraft and can be used to determine the endurance time. Results for the different propellers available for the 3D Robotics Solo and the DJI Phantom 3 were analyzed and shown how the propeller selection will affect the endurance time. Just looking at plots of the current drawn per thrust produced for different propellers is not enough to fully determine how well a propeller will perform. Knowing the thrust required to maintain flight is an important part in determining the total current the propulsion system uses.

The results presented in the paper are just the beginning of this project. The static performance data presented here and future performance data will have several uses for the design and operation of small unmanned systems. A large collection of performance information will aid in selection of the propulsion system. This performance data will also be incorporated in sUAS simulation to help provide a more realistic hands-on experience in a virtual situation.

Acknowledgments

Funding for this research was provided by the ERAU Worldwide Research Award Competition.

References

[1]FAA, https://www.faa.gov/data_research/aviation/aerospace_forecasts/media/unmanned_aircraft_systems.pdf, Accessed May 8, 2017.

[2]Elias, B., "Unmanned Aircraft Operations in Domestic Airspace: U.S. Policy Perspectives and the Regulatory Landscape," *Congressional Research Service*, 2016, pp. 1–25.

[3]Elias, B., "What a Business Aviation Flight Department Needs to Know about UAS," *Aviation Week Network*, September 25, 2015.

[4]Neubauer, K., Grosoli, F., and Verstynen, H., "Unnmanned Aircraft Systems (UAS) at Airports: A Primer," *Airport Cooperative Research Program (ACRP) Report 144*, 2015.

[5]Terwilliger B., Thirtyacre D., Ison, D., Kleinke, S., Burgess, S., Cerreta, J.S., and Walach, C., "Consumer Multirotor sUAS Evaluation and Training," *International Journal of Unmanned Systems Engineering*, Vol. 4, No. 2, 2016, pp. 1–18.

[6]Terwilliger, B., Vincenzi, D., Ison, D., Liu, D., and Kleinke, S., "Selection of optimal UAS using task requirements and platform parameters to optimize operational performance," Proceedings of the 2016 Industrial and Systems Engineering Research Conference, Norcross, GA, Institute of Industrial Engineers, 2016.

[7]FAA, "Small Unmanned Aircraft Systems Rules, 14 C.F.R. Part 107 para. 107.3," https://www.ecfr.gov/cgi-bin/text-idx?SID=e331c2fe611df1717386d29eee38b000&mc=true&node=pt14.2.107&rgn=div5.

[8]Robbins, J., Terwilliger, B., Ison, D., and Vincenzi, D., "Wide-Scale Small Unmanned Aircraft System Access to the National Airspace System," Proceedings of the Association for Unmanned Vehicle Systems International 43rd Annual Symposium, Arlington, VA, Association of Unmanned Vehicle Systems International, 2016.

[9]FAA, "Press release - FAA registered nearly 300,000 unmanned aircraft owners," https://www.faa.gov/news/press_releases/news_story.cfm?newsId=19914, January 22, 2016.

[10]Anderson, J. D., Jr., *Introduction to Flight*, 8th ed., McGraw-Hill, Inc., New York, 2015.

[11]Dole, C. E., Lewis, J. E., Badick, J. R., and Johnson, B. A., *Flight Theory and Aerodynamics*, 3rd ed., John Wiley & Sons, Inc., Hoboken, NJ, 2017.

[12]Hale, F. J., *Introduction to Aircraft Performance, Selection, and Design*, John Wiley & Sons, Inc., Hoboken, NJ, 1984.

[13]Hurt, H. H., Jr., *Aerodynamics for Naval Aviators*, https://www.faa.gov/regulations_policies/handbooks_manuals/aviation/media/00-80T-80.pdf, 1964.

[14]McCormick, B. W., *Aerodynamics, Aeronautics, and Flight Mechanics*, John Wiley and Sons, Inc, New York, 1995.

[15]U.S. Army, "Fundamentals of Flight," https://fas.org/irp/doddir/army/fm3-04-203.pdf, 2007.

[16]FAA, "Helicopter Flying Handbook," https://www.faa.gov/regulations_policies/handbooks_manuals/aviation/helicopter_flying_handbook, 2012.

[17]McCormick, Jr., B. W., *Aerodynamics of V/STOL Flight*, Dover Publications, Inc., Mineola, New York, 1999.

[18]Deters, R. W., "Performance and Slipstream Characteristics of Small-Scale Propellers at Low Reynolds Numbers," Ph.D. Dissertation, Department of Aerospace Engineering, University of Illinois at Urbana-Champaign, Urbana, IL, 2014.

[19]Deters, R. W., Ananda, G. K., and Selig, M. S., "Reynolds Number Effects on the Performance of Small-Scale Propellers," AIAA Paper 2014-2151, 2014.

[20]Carmichael, B. H., "Low Reynolds Number Airfoil Survey," NASA CR 165803, 1981.

[21]Selig, M. S., Donovan, J. F., and Fraser, D. B.,, *Airfoils at Low-Speeds*, SoarTech Publications, Virginia Beach, VA, 1989.

[22]Selig, M. S., Guglielmo, J. J. A. P. Broeren, A. P., and Giguère, P., *Summary of Low-Speed Airfoil Data*, Vol. 1, SoarTech Publications, Virginia Beach, VA, 1995.

[23]Selig, M. S., Lyon, C. A., Giguère, P., Ninham, C. P., and Guglielmo, J. J., *Summary of Low-Speed Airfoil Data*, Vol. 2, SoarTech Publications, Virginia Beach, VA, 1996.

[24]Lyon, C. A., Broeren, A. P., Giguère, P., Gopalarathnam, A., and Selig, M. S., *Summary of Low-Speed Airfoil Data*, Vol. 3, SoarTech Publications, Virginia Beach, VA, 1998.

[25]Selig, M. S., and McGranahan, B. D., "Wind Tunnel Aerodynamic Tests of Six Airfoils for Use on Small Wind Turbines," National Renewable Energy Laboratory, NREL/SR-500-34515, Golden, CO, 2004.

[26]Williamson, G. A., McGranahan, B. D., Broughton, B. A., Deters, R.W ., Brandt, J. B., and Selig, M. S., *Summary of Low-Speed Airfoil Data*, Vol. 5, 2012.

[27]Borst, H. V. and Associates, "Aerodynamic Design and Analysis of Propellers for Mini-Remotely Piloted Air Vehicles: Volume 1 — Open Propellers," USAAMRDL-TR-77-45A, 1978.

[28]Bass, R. M., "Small Scale Wind Tunnel Testing of Model Propellers," AIAA Paper 86-0392, 1986.

[29]Ol, M., Zeune, C., and Logan M., "Analytical-Experimental Comparison for Small Electric Unmanned Air Vehicle Propellers," AIAA Paper 2008-7345, 2008.

[30]Moffitt, B. A., Bradley, T. H., Parekh, D. E., and Mavris, D., "Validation of Vortex Propeller Theory for UAV Design with Uncertainty Analysis," AIAA Paper 2008-0406, 2008.

[31]sUAS Consumer Guide, http://uasguide.erau.edu, Accessed May 7, 2017.

[32]Brandt, J. B., "Small-Scale Propeller Performance at Low Speeds," M.S. Thesis, Department of Aerospace Engineering, University of Illinois at Urbana-Champaign, Urbana, IL, 2005.

[33]Brandt, J. B. and Selig, M. S., "Propeller Performance Data at Low Reynolds Numbers," AIAA Paper 2011-1255, 2011.

[34]Uhlig, D. V., "Post Stall Propeller Behavior at Low Reynolds Numbers," M.S. Thesis, Department of Aerospace Engineering, University of Illinois at Urbana-Champaign, Urbana, IL, 2007.

[35]UIUC Propeller Database, http://aerospace.illinois.edu/m-selig, Accessed May 7, 2017.

[36]Merchant, M. P. and Miller, L. S., "Propeller Performance Measurement for Low Reynolds Number UAV Applications," AIAA Paper 2006-1127, 2006.

[37]Gamble, D. E. and Arena, A., "Automated Dynamic Propeller Testing at Low Reynolds Numbers," AIAA Paper 2010-0853, 2010.

[38]Baranski, J. A., Fernelius, M. H., Hoke, J. L., Wilson, C. W., and Litke, P. J., "Characterization of Propeller Performance and Engine Mission Matching for Small Remotely Piloted Aircraft," AIAA Paper 2011-6058, 2011.

[39]Smedresman, A., Yeo, D., and Shyy, W., "Design, Fabrication, Analysis, and Testing of a Micro Air Vehicle Propeller," AIAA Paper 2011-3817, 2011.

[40]McCrink, M. H. and Gregory, J. W., "Blade Element Momentum Modeling of Low-Reynolds Electric Propulsion Systems," *Journal of Aircraft*, Vol. 54, No. 1, 2017, pp. 163–176.

[41]Justice, M., "Virtual Aerial Robotics Lab allows students to build, test, analyze from anywhere," *The Embry-Riddle Newsroom*, https://news.erau.edu/headlines/virtual-aerial-robotics-lab-allows-students-to-build-test-analyze-from-anywhere, posted 20 November 2015.

[42]Losa, M., Frendo, F. Confrancesco, A., and Bartolozzi, R., "A Procedure for Validating Fixed-Base Driving Simulations," *Transport*, Vol. 28, No. 4, 2013.

[43]Meyer, G. F., Wong, L. T., Timson E., Perfect, P, and White, M. D., "Objective Fidelity Evaluation in Multisensory Virtual Environments: Auditory Cue Fildelity in Flight Simulation," *PLos One*, Vol. 7, No. 9, 2012.

[44]Patwardhan, M. and Murthy, S., "When does higher degree of interaction lead to higher learning in visualizations? Exploring the role of 'Interactivity Enriching Features'," *Computers & Education*, Vol. 82, 2015, pp. 292–305.

[45]Potkonjak, V., Gardner, M., Callaghan, V., Mattila, P., Guetl, C., Petrovic, V. M. and Jovanovic, K., "Virtual Laboratories for Education in Science, Technology, and Engineering: A Review," *Computers & Education*, Vol. 95, 2016, pp. 309–327.

[46]3D Robotics, Inc., https://3dr.com/solo-drone/specs, Accessed May 7, 2017.

[47]Hepperle, M., PropellerScanner, http://mh-aerotools.de, Accessed May 2, 2017.

[48]Uhlig, D. V. and Selig, M. S., "Post Stall Propeller Behavior at Low Reynolds Numbers," AIAA Paper 2008-0407, 2008.

[49]Tehrani, K., "Propellers in Yaw at Low Speeds," M.S. Thesis, Department of Aerospace Engineering, University of Illinois at Urbana-Champaign, Urbana, IL, 2006.